# UC Berkeley
## UC Berkeley Previously Published Works

**Title**
Advances in nanomaterials for brain microscopy

**Permalink**
https://escholarship.org/uc/item/9546k727

**Journal**
Nano Research, 11(10)

**ISSN**
1998-0124

**Authors**
Del Bonis-O'Donnell, Jackson T
Chio, Linda
Dorlhiac, Gabriel F
et al.

**Publication Date**
2018-10-01

**DOI**
10.1007/s12274-018-2145-2

Peer reviewed

# Advances in nanomaterials for brain microscopy

Jackson T. Del Bonis-O'Donnell[1], Linda Chio[1], Gabriel F. Dorlhiac[2], Ian R. McFarlane[1], and Markita P. Landry[1,3,4,5] (✉)

[1] *Department of Chemical and Biomolecular Engineering, University of California, Berkeley, CA 94720, USA*

[2] *Biophysics Graduate Group, University of California, Berkeley, CA 94720, USA*

[3] *Innovative Genomics Institute (IGI), Berkeley, CA 94720, USA*

[4] *California Institute for Quantitative Biosciences, QB3, University of California, Berkeley, CA 94720, USA*

[5] *Chan-Zuckerberg Biohub, San Francisco, CA 94158, USA*

## ABSTRACT

Microscopic imaging of the brain continues to reveal details of its structure, connectivity, and function. To further improve our understanding of the emergent properties and functions of neural circuits, we need to directly visualize the relationship between brain structure, neuron activity, and neurochemistry. Advances in the chemical and optical properties of nanomaterials, and developments in deep-tissue microscopy, may help to overcome the current challenges of *in-vivo* brain imaging, particularly when imaging the brain through optically-dense brain tissue, skull, and scalp. Developments in nanomaterials may enable the implementation of tunable chemical functionality for neurochemical targeting and sensing, and fluorescence stability for long-term imaging. In this review, we summarize the current methods used for brain microscopy and describe the diverse classes of nanomaterials recently offered as contrast agents and functional probes for microscopic optical imaging of the brain.

## 1  Introduction

Understanding the brain and its susceptibility to injury and disease requires detailed knowledge of the structure, function, and development of a complex and dynamic system working at numerous lengths and time scales. New methods for visualizing the brain, its neurons, and their connectivity and neurochemistry will provide insight into the underlying mechanisms of brain function in its natural state (Fig. 1). Optical microscopy is a relatively noninvasive approach used to study the brain with cellular spatial resolution. Recent advances in fluorescent microscopy, including laser scanning confocal and multiphoton microscopy, have pushed the boundaries of high-resolution imaging of brain tissue. The use of fluorescent contrast agents, including organic dyes, nanomaterials, and genetically encoded proteins, has enabled us to examine the finer structure of the brain and connectivity of its neural circuits [1]. However,

---

Address correspondence to landry@berkeley.edu

large-scale whole-brain imaging with requisite spatial, temporal, and chemical resolution of neuronal and non-neuronal activity would provide a complete picture of brain function. Here, we review the advances towards this goal, the inherent challenges of using light to probe the optically-dense milieu of the brain, and the need for fluorescent probes to explore brain activity. Recent developments beyond the scope of this review, such as voltage sensitive dyes [2] and genetically encoded calcium indicators [3] for visualizing action potentials, as well as genetically encoded protein sensors for neuromodulation [4, 5], have shed light on neuronal activity. However, tools for directly examining the chemical signaling occurring between neurons in the brain extracellular space, and the activity of neuroglia, are still lacking.

Nanomaterials may address many of the challenges present in brain imaging by providing a platform for engineering chemically functional fluorescent probes for neurochemistry. The combination of neuroscience and nanotechnology over the last decade has provided numerous developments in research and clinical methods for brain science; these include drug delivery, brain imaging, and neuronal activity readout and stimulation [6, 7]. Using nanomaterials for biological imaging is advantageous because these materials are intrinsically small, ranging from 1–100 nm; this imparts these materials with unique thermal, optical, and chemical properties that differ significantly from the properties of their macroscopic counterparts. The high surface area to volume ratio provides a versatile



**Figure 1** Understanding brain function requires continued improvement and development of imaging methods to visualize the brain. (a) Physiology and structure, (b) activity and connectivity of neurons and neural circuits, and (c) dynamics of neurochemistry with requisite spatial (nm) and temporal (ms) resolution.

platform for surface modification, and can be used to engineer stability and function for targeted delivery and chemical sensing in neurological environments. Furthermore, the tunable band-gaps of semiconducting nanomaterials allow for fluorescent emission to be tuned into near-infrared (NIR) wavelengths, enabling deep microscopic exploration of living brain tissue. In this review, we summarize the latest techniques in fluorescence- and non-fluorescence-based microscopy used for imaging the brain, and highlight the burgeoning use of nanomaterials in neurobiology.

## 2 Fluorescence microscopy for brain imaging

Fluorescence microscopy, one of the most established techniques in microscopy, enables imaging of neural systems with molecular specificity. This workhorse technique is subject to continued refinements, necessitating a thorough discussion of the latest trends in brain imaging and options that influence the spatial and temporal resolution. We first discuss fluorescence excitation mechanisms, followed by a comparison of widefield epifluorescence, confocal, multiphoton, and light-sheet microscopy. We also discuss the complementary techniques commonly used for modern imaging of neural tissues, and how these techniques can benefit from the integration of nanomaterial-based fluorophores.

### 2.1 Fluorescence excitation mechanisms

Fluorescence microscopy typically makes use of chemical probes embedded within a sample. When stimulated with light, these probes emit photons of a longer wavelength and lower energy. Recently, multiphoton excitation (MPE) and upconversion excitation (UCE) of fluorescent probes have been used for *in-situ*, *ex-vivo*, and *in-vivo* neurological imaging, particularly for brain imaging. The mechanism of MPE was first predicted in 1931 [8], experimentally demonstrated in 1961 [9], and introduced for fluorescence microscopy in 1990 [10]. MPE entails the excitation of fluorophores or fluorescent nanomaterials via simultaneous absorption (Fig. 2(a)) of multiple lower-energy photons, which results in more energy than the energy of emission [11, 12]. To date, MPE has
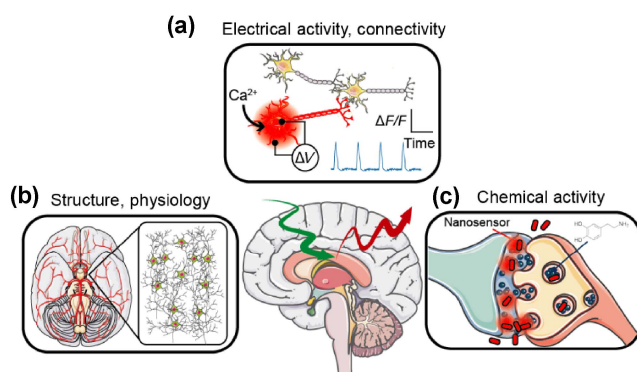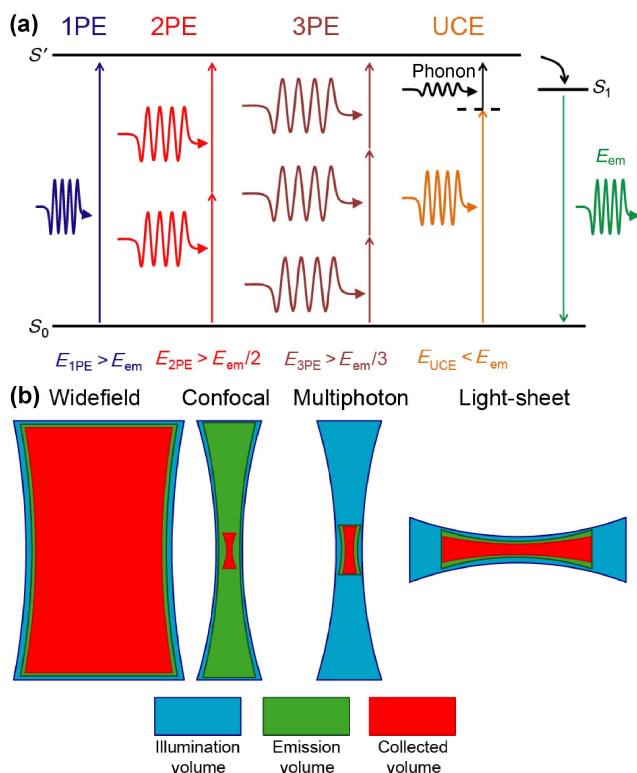
**Figure 2** Modes of optical microscopy for brain imaging. (a) Mechanism of excitation: In MPE, simultaneous absorption of photons allows an electron to be excited directly to a higher state without an intermediate electron between the ground and excited state. Shown here are examples of 2PE and 3PE, although 4PE has also been achieved. UCE involves an intermediate state that is lower than the emission energy, whereby the remaining excitation energy is typically provided by a phonon. (b) Light path diagrams of imaging modalities: In widefield microscopy, the beam fills the field of view (FOV), and the entire volume is subject to excitation and emission photons. In confocal microscopy, pinholes limit excitation volume, and the collected emission volume in the $z$-axis. The FOV is confined to a diffraction-limited spot, which is scanned across the region of interest to generate an image. In multiphoton microscopy, the light path is scanned in a manner similar to that used in confocal microscopy; however, the mechanism of MPE limits excitation volume to be smaller in $z$ than that achieved with confocal pinholes. In light-sheet microscopy, the light path travels in the same plane as FOV, providing a roughly two-dimensional sheet-shaped excitation and emission volume.

been achieved with 2-photon (2PE), 3-photon (3PE), and 4-photon (4PE) excitation modes [13].

Similar to MPE, UCE involves the absorption of photons that have lower-energy excitation than those emitted (Fig. 2(a)). Unlike MPE, UCE involves a semistable state between the excited and ground state [14–16], while true MPE involves no such states. This long-lived semistable state allows for subsequent absorption of photons, as opposed to the simultaneous photon absorption required for MPE [17]. For this reason, upconverting fluorophores can be efficiently excited at lower excitation densities than those required by MPE; this potentially minimizes tissue damage and increases the depths of image penetration into specimens such as the brain. Nanoparticles (NPs) containing a solid-state core, doped with rare earth ions, are among the most widely used UCE fluorophores, already extensively applied for *in-vitro* and *in-vivo* biological imaging [18].

## 2.2 Techniques of fluorescence microscopy

### 2.2.1 Widefield fluorescence microscopy

In widefield illumination, the traditional approach to fluorescence microscopy, the imaging plane is typically filled with photons from a defocused excitation source. This optical geometry, achieved with infinity-corrected optics by focusing the excitation source onto the back focal plane of the objective, is referred to as Köhler illumination. The image of a fluorescent specimen is focused using a tube lens and subsequently collected with a digital camera. This arrangement allows collection of both in and out of focus photons (Fig. 2(b)), producing high background levels of fluorescence, and reducing imaging contrast. This technique has the advantage of capturing a wide field of view. For imaging applications implementing bright and stationary fluorophores, widefield fluorescence microscopy is the preferred imaging modality. The relatively low cost and ease of building a flexible, customizable system render it an accessible, yet powerful, technique. For imaging deep into the brain tissue, however, the absorption and scattering of photons reduce signal strength and introduce aberrations that detrimentally impact imaging quality.

### 2.2.2 Confocal microscopy

In widefield geometries, background fluorescence, generated from scattered excitation or emission photons outside the imaging focal plane, can dramatically reduce the signal-to-noise ratio, particularly in brain tissue. To eliminate this background fluorescence, a pinhole is introduced in the excitation and emission

paths of the conjugate planes of the imaging system; this confines the excitation and collected emission volumes, respectively (Fig. 2(b)). This approach, referred to as confocal microscopy, typically features a laser scanning excitation system. A pair of scanning mirrors or an acousto-optic deflector (AOD) scans a diffraction-limited laser spot across the imaging plane, while a photomultiplier tube (PMT) or avalanche photodiode (ADP) collects the photons for each pixel. The reconstructed image can be collected for multiple vertical sections throughout a sample, producing a three-dimensional stack of the sample. This technique is limited by the speed of lateral laser scan and resolution of focal scanning. This modality is commonly used for high-resolution diffraction-limited imaging if the sample is sufficiently thin. However, high laser powers are necessary to obtain scanning speeds rapid enough to temporally resolve certain molecular processes, which can lead to tissue damage. New labeling techniques that improve fluorescence quantum yield, absorption cross-section, and photostability will greatly enhance the flexibility of confocal imaging. Nanomaterial alternatives to organic dyes, such as phospholipid nanoparticles [19], quantum dots (QDs) [20, 21], single shell QD [22], multi-shell QD [23], carbon dots [24], UCE nanoplates [16], magnetic nanoparticles [25], gold nanoparticles [26], silver nanoparticles [27], and conjugated polymer nano-particles [28], have already spurred significant improvements in confocal imaging of brain tissue.

### 2.2.3　Multiphoton microscopy

Microscopes designed to utilize MPE of fluorophores combine the advantages of confocal microscopy with tissue penetrating ability of near-infrared wavelength light. These features make MPE one of the most commonly used techniques for *in-vivo* and/or deep-brain brain imaging [29]. Because MPE of a fluorophore is a low-probability process [12], the excitation and emission volume is small in the *z*-axis compared to that of confocal microscopy (Fig. 2(b)). High peak power is necessary to excite fluorophores or luminescent probes; therefore, a pulsed laser is required to maintain low average power to avoid heating the sample [30]. This approach can be extended further into near-infrared wavelengths, which improves the depth of tissue penetration by leveraging three- and

four-photon excitation modes, but requires subsequent increases in laser power [13] and carries the risk of potential tissue heating and damage.

MPE techniques provide greater imaging depth than widefield epifluorescence microscopy, while preserving the spatial resolution of confocal imaging. The finer depth resolution allows for better resolution of *z*-scanning than that achieved with confocal or widefield microscopy, while yielding a lower fluorescence background signal; this further increases the MPE signal-to-noise ratio. At high power, 2PE can still cause out of plane background fluorescence, which can be circumvented in 3PE and even 4PE systems [13, 31]. The higher costs and limited flexibility of some commercial systems can limit the adoption of MPE for new applications. Despite these limitations, MPE microscopy, using nanomaterials as optical probes, has allowed for exceptional imaging depths and produced numerous novel techniques for brain imaging. Such developments include carbon nanotubes imaged with 2PE [32, 33], $K^+$ ion concentrations imaged with 2PE [34], quantum dots imaged with 2PE [35] and 3PE [36], gold nanorods imaged with 3PE [37], organic dye doped nanoparticles imaged with 2PE [38], and luminogens imaged with 3PE and 4PE [39]. Future studies may generate new nanomaterials that will improve quantum yield and cross-section, enabling faster scan rates. New nanomaterials may also add functionalities, such as molecular recognition, to sensing applications.

### 2.2.4　Light-sheet microscopy

Light-sheet microscopy, introduced in 2007 [40], is an approach to fluorescence microscopy in which illumination is decoupled from the optical detection pathway. This maximizes planar illumination of focal volume while minimizing potential phototoxicity [41], enabling whole-brain and whole-organism imaging. The sample is illuminated in a two-dimensional plane orthogonal to fluorescence detection (Fig. 2(b)). This provides improved signal-to-noise ratio while minimizing out of focus exposure. While geometrically challenging to engineer, light-sheet microscopy allows for rapid scanning of three-dimensional (3D) volumes, enabling whole specimen imaging and long-term exposures imaged directly onto a camera array. Recent advancements in light-sheet microscopy have

dramatically improved resolution and tissue imaging depths by incorporating other imaging modalities, such as structured illumination [42] and MPE [43]. This has allowed for direct probing of brain activity in whole animals such as zebrafish larvae and *C. elegans*.

Numerous dyes and fluorescent proteins [44, 45] have been used successfully with light-sheet microscopy. Nanoparticles have yet to make a significant impact on this imaging modality, presumably because this technique is relatively new. Ongoing advancements in highly fluorescent and stable nanoparticle probes will likely further advance light-sheet microscopy, particularly for whole-brain functional imaging at the micron scale.

### 2.2.5   *Adaptive optics*

The highly scattering nature of brain tissue introduces significant optical aberrations when reconstructing an image, which degrades image quality as imaging depths increase. This is due to the warping of excitation photons by the heterogeneous refractive index of the brain [46, 47]. Adaptive optics circumvent this issue by introducing a deformable mirror, usually based on micro-electro-mechanical (MEMS) or piezoelectric deformability, into the imaging feedback loop. The imaging wavefront, either upstream or downstream of the sample, can be corrected with the adaptive corrections of this mirror array. This increases performance and minimizes distortions, creating high-quality images and improving spatial resolution for physiological and functional deep-brain imaging. Adaptive optics were developed and implemented primarily using dyes and fluorescent proteins as optical reporters [46, 47], but can be used with multiphoton microscopy [13] as a powerful tool to improve image quality, particularly for imaging nanomaterials deep in the brain tissue.

### 2.2.6   *Sample preparation: CLARITY and expansion microscopy*

Many of the approaches described above aim to minimize the detrimental effects of tissue opacity via optical methods. CLARITY sidesteps the challenges of imaging deep into biological tissue by chemical preparation of the tissue, resulting in tissue transparency of the fixed sample. This method, developed in 2013 [48, 49], dramatically reduces tissue scattering and absorption of photons by degrading lipids, allowing for deeper imaging of relatively intact brain samples. Similar methods for such optical tissue clearing include passive clarity technique (PACT) and benzyl alcohol/ benzyl benzoate (BABB) method. For CLARITY, the proteins of an organ, such as the brain, are suspended in a gel scaffold (such as acrylamide), after which the lipids of the tissue can be washed out with lipophilic surfactants. Lipids cause the bulk of light scattering in visible wavelength imaging regime. Therefore, the resulting optically-clear brain tissue maintains an estimated 92% of its original proteins in their original configuration for high-resolution imaging [49]. This technique is used to prepare samples for confocal, multiphoton, and light-sheet microscopy [44], and is particularly well suited for light-sheet microscopy [50, 51].

Another sample preparation technique that improves imaging depth and resolution involves chemically swelling the tissue sample. Termed expansion microscopy [52], this approach physically magnifies tissue prior to imaging by chemically fixing different molecular constituents. This is followed by dialysis with water to swell the sample by more than an order of magnitude. This approach is used to image brain tissue with both light-sheet and MPE microscopy; super-resolution techniques are additionally used to image single synapses in the mouse cortex with 70-nm resolution.

While these approaches allow for molecular imaging at unparalleled depths and resolutions in brain tissue, both are post-mortem techniques, making them inapplicable for imaging dynamic cellular and molecular processes. While nanomaterials are yet to be integrated into CLARITY and expansion microscopy, deeper imaging fields with shorter integration times can be achieved with band-gap tunable and low-photobleaching nanomaterial-based contrast agents.

## 3   Nanomaterials for fluorescence microscopy

CLARITY and expansion microscopy highlight the state of the art methods for brain microscopy. However,

applications that integrate nanomaterials as contrast agents for these imaging modalities are just beginning to take hold. Engineered nanomaterials for imaging and sensing must possess several characteristics to be compatible with usage in the brain. First, they must be biocompatible, non-toxic, and colloidally stable in the complex environment of brain tissue, particularly for long-term functional imaging *in vivo*. Additionally, their surface must be chemically functionalizable to fine-tune stability, uniform distribution, and binding affinity. Fluorescence emission, either intrinsic or via chemical modification, must be stable, and any modulation to fluorescence upon binding a target should be fully reversible to enable dynamic sensing. Lastly, any binding affinity must be sensitive enough to detect endogenous concentrations of the target while maintaining selectivity. Below, we review select classes of nanomaterials (Fig. 3) that exhibit many of the above properties. We also provide recent examples of promising applications for imaging brain structure and chemistry at the microscale.

## 3.1 Carbon allotropes

The discovery of fullerenes in 1985 ushered in a new era of synthetic carbon-based nanomaterials [53].

Fullerenes are a class of molecular carbon allotropes, the simplest of which forms hollow spheroidal structures such as $C_{60}$, the buckyball. The unique chemical, electronic, and optical properties of fullerenes have fueled a "carbon gold rush", leading to the discovery and synthesis of new geometries of carbon nanostructures; these include the zero-dimensional carbon nanodot (CDot), graphene quantum dot (GQD), quasi-one-dimensional carbon nanotube [54], two-dimensional graphene [55], and other such nanostructures [56, 57]. Over the last two decades, carbon nanomaterials have been used in numerous disciplines including electronics, photonic, composites, energy storage, environmental applications, and bio-medicine [58–61]. The small size, and electronic and chemical properties of carbon nanomaterials are advantageous for developing new diagnostics and therapies in biomedicine. Functionalizing carbon nanomaterials for these applications often entails covalent tethering of polymers and biomolecules, or the adsorption of therapeutic drugs to their surface. Certain carbaceous nanoparticles, such as carbon nanotubes [62] and graphene [63–65], possess inherent photoluminescence, enabling the use of these nanomaterials for fluorescent imaging and sensing in
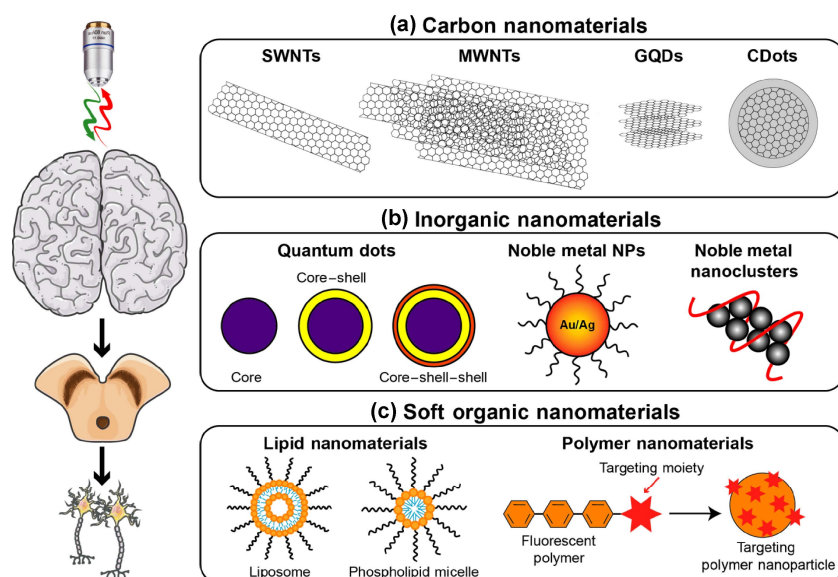


**Figure 3** Schematic representation of nanomaterials used for fluorescence imaging of the brain, ranging from whole-brain, to brain slice, to single-cell. Current and potential brain imaging applications include: (a) carbon nanomaterials, including SWNTs; MWNTs; GQDs; and CDots; (b) inorganic nanomaterials, including QDs, noble metal NPs, and noble metal nanoclusters; and (c) soft organic nanomaterials, including lipid nanoparticles and polymer nanoparticles.

tissues [66–69]. In this section, we present recent advances in some of the most studied fluorescent carbon nanomaterials and discuss their application in visualizing brain structure and function.

### 3.1.1 Carbon nanotubes

Carbon nanotubes are a diverse class of nanomaterials, with a broad range of structural and chemical forms, and resulting optical and physical properties. Carbon nanotubes are simple to chemically functionalize, which has enabled the development of gene and drug delivery platforms [59, 69]. Carbon nanotubes can also deliver drugs across the blood-brain barrier (BBB) to the brain [70]. Carbon nanotubes are especially advantageous for brain research because of their intrinsic NIR photoluminescence. Semiconducting single-walled carbon nanotubes (SWNTs) exhibit photoluminescent emission at 900–1,500 nm, falling within the NIR-II window (1,000–1,700 nm) in which photons are minimally scattered by brain tissue and minimally absorbed by water. This provides a notable advantage for improving imaging signal and resolution at depths approaching several millimeters [71–73]. Additionally, SWNTs do not photobleach; therefore, images can be collected for timescales well beyond those enabled by organic fluorophores and even by QDs [74]. The infinite photobleaching lifetime of SWNTs enables the possibility of chronic or long-term imaging studies in animal models. The first *in-vivo* experiments utilizing SWNTs for imaging in neural tissue were conducted in *drosophila* larvae by Leeuw et al. In these studies, SWNTs were incorporated into feed stock and found to distribute throughout different tissues, including the brain, with no observed short-term toxicity [75]. This result paved the way for more studies implementing SWNTs for exploring brain tissue at the cellular scale.

In their pioneering work, Dai et al. used SWNTs as imaging agents to perform precise, long-term, noninvasive imaging of cerebral vasculature through the skull of a mouse [76]. Biocompatible SWNTs have also been functionalized with a phospholipid-polyethylene glycol (PEG) construct (1,2-distearoyl-sn-glycero-3-phosphoethanolamine-N-[amino(polyethyleneglycol, 5000)]) (DSPE-PEG) and injected intravenously. By collecting SWNT fluorescence emission between 1,300–1,400 nm, Hong et al. dynamically quantified blood perfusion throughout the brains of healthy mice and those with surgically induced middle cerebral artery occlusion, achieving imaging depths in excess of 2 mm. Although restriction to the first several millimeters of brain tissue renders SWNT imaging unsuitable for most human neuro-imaging clinical applications, the noninvasive nature of this approach opens an array of possibilities for neurological imaging of awake and behaving animal models. For instance, using SWNTs in brain tissue as contrast agents can enable imaging at cellular and potentially molecular resolution in subcortical layers of the brain without the need for a chronic cranial imaging window [77].

SWNT fluorescence is also used for measuring the tortuosity of the brain extracellular space (ECS). Groc, Cognet, and colleagues demonstrated that SWNTs readily distribute throughout the extracellular space of acute brain slices obtained from rat pups [78]. SWNTs, non-covalently functionalized with DSPE-PEG, were delivered via intra-cerebroventricular (ICV) injections to several brain regions (neocortex, hippocampus, and striatum) and imaged as DSPE-PEG-SWNTs diffused through the ECS. With single-molecule localization, the authors obtained super-resolution maps of the ECS morphology with spatial resolution approaching 40 nm. The near-infrared emission of SWNTs enabled imaging depths of 100 μm into the brain slices, avoiding surface layers commonly damaged during acute slice preparation. The results of that study unveiled new complexities in ECS morphology. Obtaining data at nanometer scale in living tissue is a critical parameter for understanding extrasynaptic volume transmission, how changes in glial cell morphology impact brain function, neurodegenerative disease, and the behavior of drug molecules. Newly engineered nanomaterials, with tunable size, near-infrared fluorescence, and chemical affinity that complements established methods used for probing the morphology of ECS, will help devise new strategies for pathology and drug delivery [79–81].

In the above study, SWNTs were used in acute brain slices to study the morphology of ECS. For this SWNTs were delivered into hippocampal pyramidal cells by patch-pipetting, which showed a 1,000-fold lower diffusion constant compared to the ECS. The

large diffusion constants, measured for ICV-injected SWNTs, suggest that these nanoparticles remain primarily in the ECS and are not actively internalized into cells. This is in stark contrast to the phenomena observed in other, unrelated, studies, in which SWNT were introduced into biological systems and readily internalized into cells via passive and active mechanisms [82–85]. This can result in potentially unintended issues such as fluorescence quenching and cytotoxicity. Additionally, while the morphology of microglial cells, the brain's resident immune cells, was designated as normal in the above ECS study, microglial inflammatory responses can cause alterations in cytokine expression levels. These cellular responses should be monitored and carefully quantified at the messenger RNA or protein levels in all studies utilizing nanoparticles in brain tissue; this will ensure minimal impact on homeostatic function. It is also important to note that functionalization of nanoparticles can alter the region-specific toxicity mediated by microglia [86]. This strong toxicity dependence on the surface chemistry of nanoparticles highlights the importance of further studies on how nanoparticle surface chemistry affects their biodistribution, bio- and immune-interactions, and toxicity in living systems. Such efforts will prompt continued research into new non-covalent and covalent chemistries for controlling nanoparticle interactions with biological systems [87].

The choice of excitation source is another important factor in the implementation of SWNTs and other nanomaterials for imaging studies. Continuous wave lasers with powers exceeding 100 mW are most commonly used to excite SWNTs on-resonance at their second order excitonic transition, $S_{22}$, ranging from 600–800 nm. However, concerns over tissue health under such high fluence have motivated investigations into alternative methods of excitation. Recent studies have compared the excitation of single-chirality SWNT samples via $S_{22}$ transitions (568 nm), phonon-sideband excitation (845 nm), and upconversion (1,064 nm) [15]. Although the use of 1,064 nm laser was shown to provide the best signal-to-noise ratio for SWNT imaging in brain tissue, simulations demonstrated a 15 K increase in brain tissue sample temperature under 1,064 nm excitation. For this reason, the authors concluded that 845 nm is an optimal SWNT excitation wavelength for in-brain imaging.

Using infrared SWNTs in brain imaging has opened new directions in incorporating molecular sensing capabilities into SWNTs for dynamic imaging of brain chemistry. A new method for imparting molecular recognition elements into SWNTs preserves their NIR fluorescence by using non-covalent adsorption of amphiphilic polymers [67]. This method, termed corona phase molecular recognition, imparts molecular selectivity to the interactions between the nanotube and analyte via self-organization of the polymer adsorbate phase. To date, this approach has successfully yielded infrared fluorescent sensors for small molecules, nucleic acids, and proteins [88–91]. The creation of a turn-on NIR fluorescent nanosensor for the neuromodulatory neurotransmitter dopamine, with a fluorescent response of $\Delta F/F$ at 90%, promises to realize imaging brain neurochemistry in real-time with high spatial and temporal resolution [92, 93]. Optical imaging of dopamine with this SWNT-based dopamine nanosensor has recently been achieved in PC12 cells cultured onto a nanosensor-covered surface [94]. Recent results have shown that a highly sensitive SWNT-based catecholamine nanosensor (nIRCat), with a fluorescent response of $\Delta F/F$ exceeding 2,400% [95], can be used to image dopamine release and reuptake in living brain tissue [96]. In this latter work, the authors imaged dopamine release with nIRCats via electrical or optogenetic stimulation of acute striatal brain slices in artificial cerebral spinal fluid. The altered spatiotemporal profile of dopamine neuromodulation upon exposure to drugs was also imaged with nIRCats, by exposing striatal brain slices to dopamine-targeting agonist and antagonist pharmacological agents. These results, combined with recent analytical modeling of SWNT nanosensors for dopamine sensing [97, 98], show that these nanosensors can potentially be used *ex vivo* and *in vivo* for investigating the neurochemistry of the living brain.

Multi-walled carbon nanotubes (MWNTs), consisting of concentric cylinders of graphene, are also finding applications in brain imaging. Functionalized MWNTs have primarily been utilized for targeted delivery of therapeutics to brain tissue [99, 100]; MWNTs can cross the BBB, a highly selective, semipermeable membrane separating circulating blood from the

central nervous system. The ability to cross the BBB is enormously advantageous for nanoparticle delivery into the brain because it avoids tissue damage associated with intracranial injections. MWNTs also exhibit inherent photoluminescence, where photon emission (450–650 nm) can be stimulated using near-infrared (750–950 nm) excitation via a two-photon absorption process [101]. The photoluminescence of functionalized MWNTs was later used for multiphoton fluorescent imaging in brain tissue [33]. In that work, MWNTs were covalently functionalized with diethylenetriaminepentaacetic dianhydride (DTPA) and humanized MUC1 antibody fragment antigen-binding region (Fab'), and delivered intravenously into a mouse model. These MWNTs translocated the BBB without inflicting damage and accumulated in the parenchyma within 5 min after injection. Although this particular MWNT formulation is considered non-cytotoxic, transient inflammation (~ 72 h) was confirmed using an enzyme-linked immunosorbent assay for the inflammatory cytokine tumor necrosis factor alpha; this inflammation was minimized with a co-injection of steroidal anti-inflammatory dexamethasone, an approach that can be adopted for the use of other nanomaterials in the brain. While these results show promise, the high absorption and scattering of the visible fluorescence of MWNTs, compared with the NIR fluorescence of SWNTs, limits potential imaging applications deep in tissue.

### 3.1.2 Carbon nanodots and graphene quantum dots

CDs and GQDs are two related classes of zero-dimensional carbon nanomaterials receiving increased attention in the last decade. CDs consist of a quasi-spherical particle of carbon with a diameter below 10 nm; GQDs are particles consisting of fewer than 10 stacked layers of graphene. Both of these nano-materials exhibit tunable photoluminescence [102]. Additionally, the large surface area to volume ratio and abundance of sites for covalent modification make CDs and GQDs an ideal platform for chemical modification and functionalization. Combined with properties, such as low-photobleaching, biocompatibility, and low toxicity, these nanomaterials are considered promising alternatives to traditional fluorescent dyes for biosensing, drug delivery, phototherapy, and

bioimaging [59, 103]. Surprisingly, few examples in the literature demonstrate the potential utility of CDs and GQDs for brain imaging.

To demonstrate the advantages of GQDs for deep-tissue imaging in the brain, Qian et al. microinjected graphene oxide nanoparticles, conjugated with PEG (2,000 kDa), into the brains of mice [104]. They found that two-photon excitation of the nanoparticles, using 810-nm fs laser pulses, enabled imaging at depths reaching 300 μm into the brain tissue. The authors also note that the efficient three-photon excitation, observed in these nanoparticles, can theoretically enable even deeper tissue imaging depths and lower background, higher contrast images. Although these nanoparticles have negligible cytotoxicity, confirmed via cell proliferation assays and long-term histological comparisons, later studies suggest that similarly synthesized nanoparticles can downregulate neuronal signaling without affecting cell viability [105].

Zheng et al. synthesized CDs to enable targeted imaging of brain cancer. The resulting aspartic acid-functionalized CDs (CD-Asp) were found to be water soluble, non-cytotoxic, and emitted excitation-dependent photoluminescence ranging from 475–635 nm. Additionally, CD-Asp, delivered by tail injection, were found to readily pass through the BBB and pre-ferentially accumulate in C6 glioma cells in the brains of mice, serving as glioma-targeting imaging agents. Although the precise mechanisms for selective uptake and BBB passage remain unclear, these results show that functional CDs and GQDs can potentially be used for *in-vivo* fluorescent sensing of neurochemistry such as $Cu^{2+}$, $Ca^{2+}$, and neurotransmitters [24, 106, 107].

### 3.1.3 Nanodiamond

Nanodiamond is another carbaceous nanomaterial that can potentially be used to develop contrast agents and fluorescent probes for brain imaging and neurochemical sensing. Nanodiamonds are crystalline nanoparticles, between 2–10 nm in diameter, with tunable surface chemistry, excellent optical and mechanical properties, and lower toxicity compared with that of other nanoparticles [108]. The introduction of nitrogen-vacancy centers into the nanodiamond lattice produces stable luminescence and a long spin-coherence time, making them the most commonly used

variant for applications involving high-resolution magnetic sensing and biomedical imaging. To date, these materials have been used to quantify disease-induced changes in intraneuronal transport in cultured mouse hippocampal cells [109] and intraneuronal temperature mapping [110]. Additionally, simulation experiments show that nanodiamonds can be used to measure changes in magnetic fields, generated by axonal transmembrane potential, in imaging neural activity with high spatial and temporal resolution [111]. Although these early studies are restricted to in-culture and *in-vitro*, new vacancy engineering approaches that push nanodiamond luminescence into near-infrared wavelengths [112] may help adapt these technologies for imaging and sensing in brain tissue.

### 3.2 Inorganic nanoparticles

Inorganic nanoparticles were discovered earlier than carbon-based nanoparticles. The first examples of gold nanoparticles were actually present in ancient Roman times [113]. Semiconducting quantum dots were first mentioned in 1986 [114] and have since been extensively developed for optical imaging [115]. Two major classes of inorganic nanoparticles used in brain imaging include quantum dots and noble metal (gold and silver) nanoparticles. Both classes of these nanomaterials lend themselves to optical imaging in the brain, with properties including band-gap tunable fluorescence with minimal photobleaching, and facile chemical functionalization for targeting specific physiological and biochemical regions of a specimen. We first review the chemical and optical features of these nanoparticles, followed by recent advancements in applying these materials for visualizing brain vasculature, brain diseases, and neuronal structure.

#### 3.2.1 Quantum dots

QDs are nanoparticles composed of a fluorescent semiconducting material [116]. The nanoscale size of QDs leads to strong confinement of electrons, resulting in fluorescence properties that are tunable by altering the size or composition of the nanoparticle. QDs typically consist of a semiconducting core stabilized by either one (core–shell) or two (core–shell–shell) layers of semiconducting materials. These semiconducting layers are often hydrophobic and need to be further passivated

with ligands and polymers to enable their aqueous dispersion. QDs are ideal candidates for biological sensing because of their broadband optical absorption, easy excitation at multiple wavelengths, narrow emission bands for selective multicolor imaging, high photostability for biological imaging, and polyvalency for multifunctional applications [115, 117–121]. To better enable imaging in brain tissue, recent efforts have focused on pushing fluorescent emissions further into near-infrared wavelengths; this is achieved by developing new semiconducting materials for band-gap tuning.

Several near-infrared fluorescent QDs have been synthesized and exhibit wavelengths in the NIR-II optical window. Lead sulfide (PbS), silver selenide ($Ag_2Se$), and silver sulfide (AgS) QDs emit in the NIR or short-wavelength NIR (swNIR), and have been used for *in-vivo* imaging of mouse vasculature [122–124]. $Ag_2Se$ and AgS QDs have also shown remarkable biocompatibility. Recently, Franke and colleagues developed a method to synthesize indium arsenide (InAs) quantum dots using a continuous injection method [125]. These InAs QDs show tunable fluorescence from 900 to 1,600 nm, with the upper limit beyond the NIR window, and spanning the full spectral response of contemporary NIR detectors. swNIR-emitting InAs QDs exhibit greater chemical stability than that of PbS, $Ag_2Se$, and $Ag_2S$ QDs in aqueous media because of their unique zinc blend crystal structure. This structure allows for a more straightforward ligand exchange and coating. This stability is particularly necessary when long-term fluorescence imaging occurs in the complex biological environment of the brain. Ligands, such as small targeting peptides and PEG, can enable the delivery of QDs to specific brain regions and extend the circulation time of quantum dots [22].

InAs QDs have high quantum yields (typically 10%–20%) and narrow size distributions (core sizes of 4.3 ± 0.4 nm), allowing for deep-tissue imaging, high spatial resolution, multicolor imaging, and rapid speeds of image acquisition. These features are critical to quantifying dynamic biological processes such as neurotransmission. InAs QDs are easily functionalized and have been incorporated into phospholipid micelles, lipoproteins, and composite particles for delivery

into living animals [126]. These InAs QDs (excitation: 785 nm, emission: 900–1,350 nm) are photo- and bio-stable, and are used to image glioblastoma, a particularly malignant form of brain cancer, in mouse brains, allowing for detailed reconstruction of tumor vasculature. Imaging is conducted through a cranial window after tail-vein injection using one-photon microscopy for minutes at a time. This shows that InAs QDs can be used to image large volumes of vasculature for the pathological study of brain diseases such as stroke. InAs QDs can also be used to detect brain activation via changes in blood flow in response to external stimuli.

With respect to using QDs in brain imaging, most of the imaging experiments with QDs have been confined to the study of neural vasculature. Several obstacles prevent the delivery of QDs from blood vessels into the brain tissue for the study of brain morphology or neuronal activity at synapses. First, similar to other nanoparticles, QDs are prevented by their small size from migrating to the walls of blood vessels. QDs experience multiple collisions with larger red and white blood cells that hinder movement to the blood vessel walls [127]. Movement to blood vessel walls is a necessary step for the diffusion of particles from blood vessels into tissues via a process termed margination. Entering brain tissue from the circulatory system poses the additional challenge of traversing the BBB [128]; however, chemical methods for functionalizing QDs can be used to overcome this barrier. After crossing the BBB, probes or theranostics must also travel through the ECS. The strong fluorescence, small size, and photostability of QDs have allowed for precise optical measurements of ECS in living rat neocortex, providing details on endogenous spread of neurotransmitters and diffusion of exogenous agents [129].

Noninvasive imaging of brain tumors has recently been accomplished with QDs decorated with targeting peptides that traverse the BBB. Huang and colleagues functionalized CdSe/ZnS QDs (excitation: 488 nm, emission: 525 nm) with an asparagine-glycine-arginine (NGR) peptide and PEG to create NGR-PEG-QDs that localized to glioma brain tumors [22]. The NGR peptide specifically targets a type II transmembrane glycoprotein (CD13) overexpressed on the surface of glioma cells, whereby surface functionalization with PEG increases the circulation time of these QDs. These NGR-PEG-QDs were injected into mice via tail-vein injection and were shown to localize into brain tumors after 8 h. This localization into brain tumors is driven by targeting ligands and potentially increased permeability of tumor vasculature. In future work, the development of a more general delivery method will help bypass the BBB for brain imaging in cancer-free systems and for imaging homeostatic brain activity [130].

Functionalization of surfaces using ligands can also be used to distinctly tune the physical properties of QDs; this affects the localization and application of these nanoparticles [131]. Recent work has shown the importance of negative surface charge on QDs. Within minutes, QDs with a negative surface charge preferentially and specifically localize to the membranes of neuronal cells over glial cells [132, 133]. Surface charge, as opposed to the size, shape, or composition of QDs, is a prevailing factor in internalization. This is due to QD interaction with the bioelectrical surface of the neuron. This recent work contradicts previous findings, which show nonspecific uptake of QDs by glial cells independent of surface charge and functionalization [134, 135]. More research into the physical properties and subsequent function of QDs is necessary; however, these findings indicate the possible approaches for future design of targeting QDs for brain imaging.

To circumvent the barrier of diffusion through the BBB, QDs can also be injected directly into the brain. Using high osmolarity solutions to temporarily open BBB junctions or by performing direct intracerebral injections [136,137], imaging contrast agents can be introduced into the brain. Although intracerebral injections are used ubiquitously for the administration of drugs and therapies to brain tissue, precise localization is a challenge and limited diffusion can impact distribution. Additionally, injections can locally activate glial cells, triggering an inflammatory response that may complicate experimental results. Alternatively, injections directed into the brain ventricle, the cavity of the brain where cerebrospinal fluid is housed, show relatively low activation of microglia [20]. The ventricular area is one of the more permissive barriers

for delivery into the brain, making it a promising approach for introducing QDs and other nano-materials into functional regions of the brain [128]. Using ventricular injections, antibody–QD conjugates (excitation: 561 nm, emission: 655 nm) have been employed to label single-dopamine receptors for single-receptor diffusion tracking in acute brain slices. This method of direct injection is not unique to QDs, and can be used to deliver other nanoparticles directly into the brain without having to pass the BBB.

Another challenge in the study of neuronal activity occurs once the QDs are delivered into the brain. The large hydrodynamic size of many commercially available and/or colloidally suspended QDs (~ 30–100 nm), relative to the size of neuronal synapses (~ 30 nm), often prevents the imaging of synaptic features. However, recent methods in QD synthesis enable the tunable synthesis of small-diameter QDs, which can access synaptic clefts and are now available commercially with PEGylation [138]. Cai and colleagues synthesized stable small quantum dots (sQD, excitation: 488 nm, emission: 527 or 615 nm) that possess 9-nm diameter cores and thin ligand layers [139]. These sQDs can be labeled with streptavidin and can bind biotin-labeled AMPA receptors in two live-rat primary neuronal cell lines. The sQDs are imaged using super-resolution microscopy photoactivated localization-fluorescence imaging with one-nanometer accuracy (PALM-FIONA) system. Diffusion of AMPA receptors is quantified by tracking sQDs within synapses. Single quantum dot tracking has been used to study numerous different types of synaptic receptors [140, 141], providing insight into changes in synaptic plasticity. This is the first step towards visualizing the dynamic processes associated with neural activity. In fundamental neurobiology, QDs, loaded into cultured hippocampal vesicles, are used to visually confirm and quantify the controversial concept of kiss-and-run versus full collapse fusion of neurotransmitter-loaded vesicles at pre-synaptic boutons [142]. Although powerful, these methods are only used to indirectly visualize neurochemistry in cultured cells. Future work will likely address their implementation *in vivo*.

Another approach to infer neural activity is by quantifying changes in neuronal membrane potential, which governs neurotransmitter release and chemical communication between cells following action potential. QDs offer several advantages over alternative methods, namely voltage sensitive dyes and genetically encoded fluorescent proteins. This is because QDs are brighter, more photostable, and can be engineered to exhibit great changes in fluorescence as a function of voltage with rapid temporal responses [143, 144]. Further tailoring these QDs to localize into plasma membranes has resulted in superior fluorescent responses to changes in membrane potential. This has been shown in HeLa cells, PC12 cells, and in anesthetized adult mice *in vivo* [145]. CdSe/CdS/ZnS nanoparticles (emission at 600-650 nm), functionalized with peptide and fullerene molecules, have been introduced by intracortical injection into the parietal cortex of the brain and imaged at the depth of 100 μm using 460–520 nm light stimulation. Electrical stimulation is used to modify cell membrane potentials while monitoring the fluorescence response of these QDs. Although these QDs provide a superior fluorescent signal compared to available voltage dyes, it remains to be seen whether this method can be used to study endogenous neuronal firing *in vivo*.

Many studies focus on neuronal activity, but the function and activity of non-neuronal structures remain important components in understanding the overall function and health of the brain. Neuroglial cells, comprised primarily of microglia and astrocytes, are the resident immune cells of the brain, and function in concert with neurons to modulate brain activity. QDs have been implemented to track the glutamate transporter GLT-1 on the membrane of astrocytes, revealing that the diffusion of GTL-1 dictates glutamate clearance rates near synapses, thus shaping neuro-transmission [146]. Such long-term fluorescent imaging, enabled by the robust photostability of QDs and other nanomaterials, can provide important insights into the dynamic interactions between neural and glial cells at molecular level. This can provide new insights into their roles in neurological and psychiatric disease.

Although the use of QDs has made tremendous strides in the *in-vivo* imaging of brain tumors, imaging neuronal vasculature, neuronal receptors, and neural electrical activity remains challenging. As synthesized, QDs are not biocompatible and require ligand functionalization that is not necessarily straightforward,

particularly if it requires combining multiple functionalities. There is also a concern of heavy metal toxicity from QDs during long-term *in-vivo* imaging [147, 148]. Accumulation of QDs in the body can result in oxidative breakdown of the nanoparticle in the lysozyme of the cell, causing toxicity induced by reactive-oxygen species [149–151]. These challenges in functionalization and stability need to be addressed before using quantum dots to image the spatiotemporal dynamics of electrical (action potential) and chemical (neurochemical and neuromodulatory) activity of the brain.

### 3.2.2    *Noble metal nanoparticles*

Noble metal nanoparticles, including gold and silver nanoparticles, exhibit numerous physical and chemical advantages that lend themselves to biological and imaging applications. Because of their lower toxicities, these nanoparticles are extensively used to create probes for imaging, therapeutics, and theranostics [152, 153]. However, noble metal nanoparticles are less frequently used with fluorescence microscopy because of their weak intrinsic photoluminescence [154] and propensity to quench fluorescent dyes. Despite this limitation, several applications for brain imaging have been realized with noble metal nanoparticles, highlighting their potential use as multifunctional fluorescent probes. Gold nanoparticles (AuNPs) exhibit strong surface plasmon resonance, the coherent oscillation of surface conduction electrons excited by the electromagnetic field of incoming light. Surface plasmon resonance leads to powerful fluorescence, and surface-enhanced Raman scattering (SERS) properties of AuNPs are used in optical imaging applications [155]. Surprisingly, fewer applications of AuNPs have been translated to optical brain imaging, although AuNPs have been used in several non-optical methods of detection such as magnetic resonance imaging (MRI), positron emission tomography (PET), and computed tomography (CT) [156–158]. Because AuNPs show numerous features attractive for imaging, many reports on AuNPs involve theranostics, the coupling of therapeutics and diagnostics using the same nanoparticles [159, 160]. AuNPs do not tend to have intrinsic fluorescence, but are readily used for imaging and brain imaging after conjugation with

fluorescent moieties and stabilizing of functional ligands.

Delivery of AuNPs is critical for their eventual adoption in brain imaging. A study on biodistribution of colloidal AuNPs after intravenous administration showed that AuNPs, smaller than 50 nm in diameter, diffused through the BBB [161]. Alternatively, the delivery of AuNPs to the brain via olfactory pathway was another successful strategy [162]. In that study, AuNPs, labeled with fluorescein (excitation: 490 nm, emission: 525 nm), were fluorescently imaged in the central nervous system of locusts upon olfactory delivery. These AuNPs, with a mean diameter of $13.22 \pm 1.19$ nm, were shown to passively diffuse through the BBB within 1 h of olfactory exposure. This method of delivery to the brain is less invasive compared with injection methods described in the previous sections. However, more studies need to determine how physical attributes, such as size, charge, and shape, govern the successful delivery of AuNPs and other nanomaterials to the brain via olfactory pathway.

AuNPs can quench the fluorescence of fluorophores that are in close proximity to the surface of the nanoparticle. This occurs via energy transfer, enabling the design of functional fluorescent sensors. Phthalocyanine 4 (PC4) is an intrinsically fluorescent hydrophobic photodynamic therapy drug for glioblastoma multiforme, one of the deadliest forms of brain cancer. PC4 can be adsorbed on the surface of AuNPs via a terminal amine group [163]. Upon adsorption to the surface of AuNPs, the fluorescence of PC4 at 685 nm is quenched, and only release of the drug from the nanoparticle upon illumination with light recovers the fluorescence. This approach has enabled fluorescent quantification of drug release in tumors, as shown in brain slices excised from mouse models.

AuNPs are easily surface-modified with ligands to improve colloidal stability and to target specific organs or tumors. This is a useful approach, adaptable to targeting particular neural subsets or brain regions. The gold surface readily forms strong bonds with thiolated chemicals that enable the tethering of targeting moieties such as antibodies, targeting peptides, and fluorophores. AuNPs have higher retention in brain

tumors after *in-situ* enzyme-induced aggregation [26]. AuNPs conjugated with Ala-Ala-Asn-Cys-Lys peptide, and 2-cyano-6-amino-benzothiazole-modified AuNPs, can be hydrolyzed by legumain to form fluorescently labeled aggregates. Legumain is a protein involved in hydrolysis and found at disproportionately high concentrations in brain tumors. These aggregates can be prelabeled with Cy5.5 fluorophores, enabling selective fluorescence imaging of brain tumors.

Gold nanorods (GNRs) possess the many attractive properties of AuNPs but with a strong longitudinally localized surface plasmon resonance (LSPR) band, tunable from visible wavelengths to NIR. Additionally, GNRs exhibit strong plasmon-enhanced multiphoton luminescence with a brightness that rivals that of common organic fluorophores [164]. To adapt GNRs for deep *in-vivo* brain imaging, Wang et al. modified a conventional seed-mediated synthesis to create large aspect ratio GNRs (100 nm in length) having LSPR peaks at 1,000 nm, which is within the tissue transparency window for imaging the brain [37]. Using a femtosecond pulsed laser, these GNRs were found to emit broadband multiphoton luminescence (420–630 nm), stemming from a combination of two-photon and three-photon excitation, without any observable photobleaching. After passivation using PEG, these GNRs were intravenously injected into mice. High-resolution imaging of brain blood vessels was achieved with extremely low background fluorescence at depths reaching 700 μm into brain tissue. The highly sensitive nature of LSPR, and the ease of functionalizing their surface, renders GNRs a promising platform for future work such as imparting molecular recognition to functional chemical probes and investigating function in living brain tissue.

Silver nanoparticles (AgNPs) are photostable, non-photobleaching, and highly scattering nanoparticles that are increasingly used in brain imaging. Several key optical imaging methods have been used to image the brain with AgNPs as the optical probes. In one application, highly scattering AgNPs (initially 35.4 ± 5.3 nm) were imaged *in vivo* in glioma brain tumors using darkfield microscopy on a confocal microscope [27]. AgNPs were entrapped in a poly(lactic-co-glycolic acid) (PLGA) polymer nanoparticle and conjugated

to cholorotoxin peptides that selectively bound to glioma cells. These AgNP-PLGA constructs, with a final size of 114 nm (± 2 nm), were injected into a mouse via the tail-vein, permeabilized through the BBB, and aggregated in glioma tumors. The AgNPs within the PLGA nanoparticle served as contrast agents, which eliminated the need for nanoparticle surface modifications that can impact the behavior of the nanoparticle *in vivo*.

Another class of silver nanoparticles, silver nano-clusters (AgNCs), are composed of a few-atom core of silver atoms and ions stabilized by a polymeric ligand. These clusters show promise for numerous biological applications because of their small size (< 1 nm), superior optical properties and biocompatibility [165, 166]. Recently, AgNCs stabilized by short DNA strands have been shown as effective fluorescent sensors of neurotransmitters such as dopamine [167]. The fluorescence of select DNA-AgNCs, with fluorescence emission wavelengths approaching 800 nm, can either increase or decrease upon the addition of dopamine either pre-synthesis, for *in-vitro* sensing, or post-synthesis, for potential *in-vivo* sensing. These results highlight the potential of using DNA-AgNCs as a platform for engineering selective, sensitive, ratiometric fluorescent sensors for direct fluorescent sensing of neurotransmitters. With reversibility studies and further validation of their biocompatibility in brain tissue, these small AgNCs can enable *in-vivo* fluorescence imaging of neurotransmission at and around synaptic connections.

Noble metal nanoparticles, including AuNPs and AgNPs, have been well characterized for optical imaging in biological systems, and have found some applications in brain imaging. AuNPs have been studied extensively, optimized for biological delivery, and can be coupled to fluorescent drugs or fluoro-phores for fluorescent or darkfield imaging of brain tissue. Recent efforts, focused on using noble metal nanoparticles as neurotransmitter sensors, may develop methods for the *in-vivo* imaging of neurochemistry. Although widely regarded as biocompatible, more studies need to characterize the longevity and clearance of noble metal nanoparticles for use in long-term brain imaging studies.

### 3.3 Soft organic nanoparticles

Organic nanoparticles, such as lipid-based [168] and polymer nanoparticles [169], dubbed "soft" nano-materials, have recently gained popularity in fluorescent imaging applications [170]. Since the discovery of the liposome in the mid-1960s, these amphiphilic nanoparticles have ushered major advancements in therapeutic drug delivery via stable encapsulation of highly hydrophobic drug molecules. Organic nano-particles are accompanied by fewer biocompatibility issues than are their inorganic counterparts. This is because organic nanoparticles are composed of biodegradable monomers that can be cleared from the body [171]. These organic nanoparticles can be intrinsically fluorescent, as in the case of fluorescent conjugated polymers, or via encapsulation of a fluorophore. Although there are benefits to using fluorescent soft organic nanoparticles for bioimaging, particularly for the imaging of brain tissue [172], there are few examples of such use. Here, we review lipid-based and polymer-based nanoparticles, the two major classes of organic nanoparticles, and discuss their potentials in brain imaging:

#### 3.3.1 *Lipid-based nanomaterials*

Lipids have the ability to encapsulate organic dyes and fluorescent nanoparticles to create biocompatible fluorescent nanoparticles and nanodroplets. The liposomes and micelles created in lipid formulations are often resistant to degradation at different pH and in harsh chemical environments [173]. Lipid encapsulation localizes multiple organic fluorophores into the nanoparticle core, resulting in a particle with higher fluorescence signal than that of a singular fluorophore. Lipid encapsulation can also circumvent the insolubility of many organic fluorophores by encapsulating fluoro-phores in a hydrophilic particle with a hydrophobic core [174].

This technique of lipid encapsulation was employed in the NIR fluorescent imaging of brain tumors using a hydrophobic heptamethine cyanine (IR780) fluoro-phore (excitation: 745 nm, emission: 815 nm) [19]. The fluorophore was encapsulated into liposomes and phospholipid micelles; the size of the particles was selectively and accurately tuned by changing the lipid formulation via ratio of different phospholipids and cholesterol. IR780 has inherent brain tumor-targeting abilities. Thus, encapsulating in lipid nano-particles allowed for accumulation of micelles in brain tumors after tail-vein injection. Hong and colleagues used a similar technique to encapsulate fluorescent conjugated polymer nanoparticles with a quantum yield of 1.7% and tunable emission from 1,050–1,350 nm, falling within the NIR-II region of biological trans-parency window. These nanoparticles show high resolution and can be used for deep-tissue imaging of mice vasculature, improving the image quality compared with that achieved by traditional ultrasound and computed tomography. The fluorescence emission of these nanoparticles makes them well suited for deep-tissue brain imaging, particularly if they can be engineered as chemical probes.

#### 3.3.2 *Polymer-based nanoparticles*

Polymer-based nanoparticles are synthesized in two forms: fluorescent conjugated polymer nanoparticles and polymer-encapsulated fluorescent moieties. To date, only fluorescent conjugated polymer nanoparticles and dendrimer-encapsulated fluorophores have been used for brain imaging.

Fluorescent conjugated polymers have been shown to self-assemble into nanoparticles, which are used for neurotransmitter sensing. Conjugated copolymers of fluorene and benzothiadiazole are coupled to phenylboronic acid tags (PFPBA) to create highly sensitive, selective, and photostable fluorescent dopamine sensors (excitation: 309 and 419 nm, emission: 529 nm) [28]. The phenylboronic acid acts as a recognition ligand that specifically binds to dopamine over other neurotransmitters. This copolymer for-mulation can self-assemble into spherical nanoparticles by solvent exchange, which promotes formation of a hydrophobic core surrounded by a hydrophilic shell, resulting in nanoparticles of 120 nm in diameter. The authors observed no significant cytotoxicity or cell death with the concentrations of nanoparticles used in the study. These nanoparticles were used to image dopamine in PC12 cells *in vitro* and in zebrafish larvae *in vivo* with confocal microscopy. Because of

the lack of a fluorescent baseline, this polymer nano-particle cannot detect endogenous dopamine levels but can successfully measure exogenous dopamine added to the brains of zebrafish larvae. Further improvements to recognition chemistry may provide future fluorescent sensors for other neurotransmitters, expanding the range of compatible neural probes.

Dendrimers are monodispersed multibranched polymers with recent applications in brain imaging. Although not inherently fluorescent, dendrimers have been used to encapsulate or covalently tether fluorescent molecules for imaging. Of note, PEG-functionalized poly(amidoamine) (PAMAM) dendrimers have been used to encapsulate ion-sensitive fluorescent dyes for the detection of important neuronal ions including potassium and sodium in brain slices [34, 175]. Dendrimers are ideal candidates for optical imaging in the brain because certain formulations can traverse the BBB. Once internalized into the brain ECS, dendrimers can be uptaken by neurons and glial cells, while the dendrimeric formulation protects the fluorescent dye cargo from triggering immune responses or interfering with receptor–antagonist interactions of neurotransmitters [176–178]. More research into ligand decoration of dendrimer surfaces, and improved control of the growth of dendrimer structure, can further promote their use in optical imaging.

Organic nanoparticles provide a facile scaffold for creating fluorescent imaging probes. The monomeric components of organic nanoparticles are smaller than the hydrodynamic cutoff of 5.5 nm, resulting in effective renal excretion from the body [179]. However, these nanoparticles often encapsulate fluorescent loads, such as hydrophobic dyes and quantum dots, which cannot be excreted renally. This may lead to long-term cytotoxicity. Fluorescence-conjugated polymers can also suffer from loss of fluorescence, which originates from the chemical coupling of a ligand required for molecular recognition or targeting. Although polymeric nanoparticles are difficult to synthesize, they enable tunable surface properties such as hydrophilicity and hydrophilicity, grafting of targeting moieties, and possess sizes that are amenable for brain imaging.

# 4  Non-fluorescence imaging methods in the brain

## 4.1  Imaging vibrations: SERS

In addition to fluorescence, a number of other optical processes have been gaining popularity in brain imaging applications. These include vibrational spectroscopies such as Raman scattering and infrared (IR) absorption. Vibrational spectroscopies are optical techniques that measure the vibrational modes of molecules, typically via direct absorption of IR light or inelastic scattering of incident light (Raman). Vibrational modes are specific to bonds and functional groups, thus providing information on the chemical composition of a sample. Vibrational imaging is attractive because it provides spatially resolved and chemically specific information, often without the need for molecular labeling with fluorescent dyes. However, vibrational spectroscopies, such as Raman scattering and IR absorption, also have disadvantages when used for imaging. IR absorption has low spatial resolution due to the long wavelengths used (3–100 μm). Difficulties also arise from the strong absorption of water in this wavelength region. For this reason, Raman scattering, which is the inelastic scattering of photons due to vibrations in the sample, is often preferable because it can be performed with visible or near IR illumination. However, this process has very low scattering cross-sections, requiring higher laser powers and long times of image acquisition. One method, used to circumvent the challenges of low signal-to-noise ratios, implements SERS using plasmonic nanomaterials.

In spontaneous Raman scattering, light of frequency $\omega_i$, incident on a molecule, excites that molecule to a virtual excitedstate, whereupon the molecule relaxes to an excited ground vibrational state, releasing a photon of lower frequency $\omega_i - \omega_v$; $\omega_v$ is the frequency of the vibration (Stokes scattering) (Fig. 4(a)). If the molecule was already in an excited vibrational state, the incident photon can gain energy from the vibration, and be released at frequency $\omega_i + \omega_v$ (anti-Stokes scattering), returning the molecule to the ground state. In SERS, the same process takes place; however, a large cross-sectional increase occurs as the effective
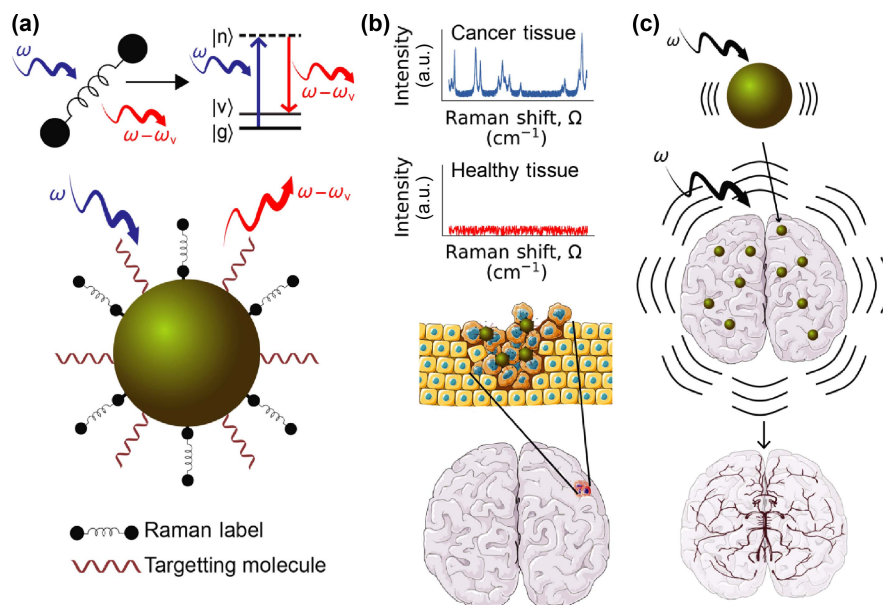
**Figure 4** Raman-based brain imaging. (a) Raman scattering and surface-enhanced Raman scattering: Raman scattering is the inelastic scattering of light due to molecular vibrations. At room temperature, most compounds are in their grounded vibrational state. The inelastically-scattered light is of lower energy than incident light, with the energy difference corresponding to the energy of the molecular vibration (left). Raman scattering is an infrequent process; however, the use of plasmonic nanomaterials (right) results in a local field enhancement via SERS, resulting in a signal increase and faster imaging rates. For brain imaging applications, Raman-active probes are usually affixed to plasmonic nanoparticles (e.g., AuNPs) (right). (b) SERS probes for brain cancer imaging: SERS probes, labeled with specific Raman-active molecules, can be used for brain imaging to detect brain tumors. Cancer cells are specifically targeted via functionalization of SERS probes with targeting molecules, or by exploiting the "enhanced permeability and retention" effect, where cancer cells more readily uptake and retain nanomaterials. Detection of the Raman-active molecule signature indicates cancer (top spectrum), whereas lack of signal indicates healthy tissue (bottom spectrum). (c) Photoacoustic imaging: The photoacoustic effect, where absorption of light results in thermoelastic expansion, can be exploited for Raman imaging. Certain nanomaterials, such as gold nanoparticles (top), possess large photoacoustic efficiencies, which provide strong imaging contrast over large areas. Introduction of nanoparticles can, therefore, be used to construct tomographic reconstructions of large segments of brain morphology such as the vasculature (bottom).

local electric field around a nanomaterial is increased from the excitation of surface plasmons [180]. The scattered photon energy loss or gain still occurs in response to the vibrations of the molecules near the nanomaterial. The nanomaterial functions solely as an "antenna", enhancing the vibrational signals coming from its local environment.

Historically, SERS has been used to study the chemical composition of samples or their vibrational properties; however, as applied in neural imaging, SERS probes are frequently functionalized with a Raman-active probe and/or a molecule to specifically localize the probes to a cell type. Often, Raman-active probes are developed for bioimaging via introduction of functional groups containing vibrational frequencies in the "cell-silent" region of the spectrum, which

corresponds to ~ 1,800–2,800 cm$^{-1}$. This window is chosen because the bonds in biological molecules vibrate at either higher or lower frequencies, providing a considerable spectral region where exogenous signals can be introduced without biological background. The probe is then imaged by specifically looking for a Raman shift in this window. This is less of a concern when labeling SERS nanoparticles because SERS signal enhancement allows for rapid collection of the entire Raman spectrum of a probe with high spectral resolution. As a result, nanoparticle–Raman–probe conjugates used for brain imaging are developed to have unique Raman spectra, but do not necessarily contain modes within the cell-silent region.

One potential obstacle of SERS in neural imaging is that local field enhancement only occurs in the direct

vicinity of the nanoparticle. Therefore, signal uniformity can vary greatly when imaging over large sample areas. Lithographic techniques can be used to generate periodic arrays of structures. However, these techniques are technically challenging to incorporate into brain imaging. Addressing this drawback, Yamazoe et al. [181] synthesized gold nanoparticles on a random nanostructure of boehmite. The resultant random "gold nanocorals" featured ~ 125 nm diameter AuNPs spaced at 10 nm or less. This is sufficient for maintaining local field enhancement, while greatly increasing the homogeneity of signal collection over a large surface area. Yamazoe and colleagues demonstrated the utility of this system in ischemic mouse brain slices, where ischemia was induced by middle artery occlusion. The authors determined the boundaries of the affected area with SERS imaging at two vibrational peaks, with one corresponding to adenosine (736 cm$^{-1}$) because ischemia causes the breakdown of ATP into constituent metabolites.

As is the case with other types of nanoparticles, cytotoxicity and distribution are a concern when using SERS probes for *in-vivo* imaging. In 2010, Wang et al. [182] demonstrated the feasibility of using SERS probes in zebrafish embryos. In that study, AuNPs were conjugated to mercaptobenzoic acid, a non-fluorescent Raman label that has unique vibrational signatures. The authors injected 5 nM SERS probes with conjugated labels into the one-cell stage of the embryo and tracked embryonic development over 7 days. During the fully developed stage, SERS signals were recovered from the fore and hindbrain of the zebrafish. This study demonstrated that the morphological development of zebrafish, injected with SERS probes, was indistinguishable from that of the wildtype. Furthermore, the authors demonstrated the ability to simultaneously track SERS probes with two different Raman labels, mercaptobenzoic acid and mercaptopyridine, with vibrational signatures differing by ~ 50 cm$^{-1}$, less than the linewidth of a typical fluorescent signal.

In an alternative strategy, Diaz et al. [183] used MRI-guided focused ultrasound to deliver silica-encapsulated AuNPs across the BBB for the purpose of studying glioblastoma in rat brains (Fig. 4(b)). Specific targeting of SERS probes to glioblastoma cells

was accomplished by functionalization with anti-EGFR (epidermal growth factor receptor) antibody. This is because EGFR is highly expressed in cancer. Nanoparticles injected via the tail vein were visualized in the brain parenchyma after focused ultrasound, but not solely after injection. Specific uptake of anti-EGFR SERS probes by tumor cells was verified in cultured cell lines. Particle retention was also shown in human glioblastoma cells after xenograft into the mouse brain. These methodologies and results indicate the potential utility of SERS nanoparticles in studying brain cancer.

SERS nanoparticles have been used by other groups to study glioblastoma. Karbeber et al. used a handheld Raman scanning device to demonstrate the potential clinical application of silica-encapsulated AuNPs to guide glioblastoma tumor resection in mice [184]. Tumor uptake of the nanoparticles was confirmed by transmission electron microscopy (TEM) and immunohistochemistry. The success rate of the resection was higher than that achieved with simple white light visualization and was comparable to detection abilities of traditional Raman microscopy. The use of the handheld scanner improved acquisition speeds by several orders of magnitude, rendering it a viable alternative to real-time brain-tumor imaging in a clinical setting.

The Kircher group extended this work by developing and implementing surface-enhanced resonant Raman scattering (SERRS) probes [185]. SERRS rely on the linking of SERS nanoparticles, in this case gold nanospheres or nanostars, to a Raman label, which is in electronic resonance with the excitation laser, in this case IR792 perchlorate (for the nanospheres) or IR780 (for the nanostars). The electronic resonance of the Raman reporter provides multiple additional orders of magnitude in signal enhancement, leading to detection sensitivities in the femtomolar range. The IR792 construct was integrin-targeted (RGD-SERRS), and the IR780 construct served as control (RAD-SERRS). These constructs were injected at an equimolar ratio into a mouse tail vein prior to imaging. Both were found throughout the brain, although the RGD-SERRS showed several orders of magnitude higher signal intensity in tumor regions than that of RAD-SERRS. Additionally, RGD-SERRS allowed detection of

microscopic glioblastoma invasions beyond the site of the main tumor, where RAD-SERRS was not detected.

## 4.2   Imaging vibrations: Nonlinear Raman microscopy (surface-enhanced coherent anti-stokes Raman scattering (SECARS))

Nonlinear optical techniques require costly pulsed lasers and additional optics to enable label-free imaging. However, nanomaterials used in conjunction with nonlinear optical techniques can enable additional functionality over their label-free counterparts. One such example, a nonlinear variant of SERS, is SECARS. SECARS has been applied in brain imaging using iron oxide nanoparticles [186]. SECARS is based on coherent anti-stokes Raman scattering (CARS), a four-wave mixing technique that uses two incoming pulsed lasers of frequencies $\omega_p$ and $\omega_s$, where $\omega_p - \omega_s = \omega_v$ is the frequency of some molecular vibration in the sample, with the emitted photon being released at the frequency $\omega_{as} = 2\omega_p - \omega_s$. This process already provides strong signal enhancement compared to that of spontaneous Raman scattering, but can be surface enhanced when any of the three frequencies, $\omega_p$, $\omega_s$, or $\omega_{as}$, excite plasmon resonances in a nearby nanomaterial.

Machtoub et al. used ultra-small paramagnetic iron oxide particles (USPIOs), labeled with anti-CD4, in a rat model of amyotrophic lateral sclerosis. USPIOs are well-known MRI contrast agents, allowing for direct image comparisons with SECARS. The results of SECARS imaging indicated enhancement of lipid-associated vibrations in the vicinity of USPIOs, which correlated with areas of inflammatory response due to the anti-CD4 labeling of USPIOs. These data showed lipid and iron accumulation in areas associated with amyotrophic lateral sclerosis.

## 4.3   Imaging absorption: Photoacoustic imaging (PAI)

Optical imaging tools have high spatial resolution and can possess high chemical specificity. However, optical imaging typically suffers from low penetration depths in biological tissues due to the highly scattering nature of biological tissues. Photoacoustic microscopy and tomography (PAM and PAT; or PAI) are recently-developed hybrid biomedical imaging tools that use optical excitation, typically with ns pulsed lasers and ultrasonic detection [187]. These techniques can be used to measure thermoelastic expansion caused by optical absorption, providing molecular specificity based on absorption. These methods also show deep-tissue penetration because of low scattering of the released ultrasonic waves. While the spatial resolution of PAI is not as high as that achieved by purely optical techniques, the penetration depth is greater than that achieved by fluorescence microscopy, and whole-brain images can be collected in rodents (Fig. 4(c)). Additionally, spatial sensitivity can be improved by using certain classes of nanomaterials as contrast agents.

In 2010, Lu et al. implemented PAI with hollow gold nanospheres (HAuNS) to image the brain vasculature [188]. HAuNS, which are 45-nm spheres with a hollow interior and 4-nm thickness of the gold shell, absorb at 800 nm in the NIR to maximize the depth of optical penetration. The hollow interior increases absorption coefficients, while decreasing scattering coefficients. When coated with PEG, HAuNS can be injected intravenously and used to visualize brain vasculature. HAuNS enable the resolved imaging of blood vessels 100-μm in diameter in whole mouse brains. Of note, limited toxicity to the liver, spleen, and kidneys are observed via immunohistochemistry in animals injected with HAuNS.

PAI is also used in clinical contexts for imaging brain-tumor boundaries. Ray et al. developed nanoparticles synthesized from polyacrylamide hydrogels with conjugated Coomassie Blue dye. These nanoparticles were further functionalized with a tumor-targeting peptide [189]. *Ex-vivo* effectiveness of PAI-based imaging using these nanoparticles was demonstrated in brains excised from rats implanted with 9L glioma. The tumor-targeted nanoparticles showed clear PAI contrast in the regions of implantation. However, Coomassie Blue, with a 590-nm maximum absorption wavelength, is not the best dye for *in-vivo* applications because of the strong absorption of blood in the visible wavelength range.

In another example of tumor imaging, Fan et al.

developed perylene-diimide based nanoparticles for NIR PAI of tumors in the brain [190]. The perylene-diimide molecules were encapsulated with DSPE-methyl-PEG(5,000 kDa), creating nanoparticles ~ 48 nm in diameter, with a maximal absorption wavelength of 700 nm. These nanoparticles were shown to be chemically stable in phosphate buffered saline and mouse serum, and largely photostable under an hour of continuous illumination. Detection sensitivity was assessed with subcutaneous injection of the nanoparticles into the lower back of mice. A linear concentration dependence was observed for the signal, with tissue background detection limit at sub-nM concentrations. Interestingly, when these nanoparticles were used for brain-tumor imaging after tail-vein injection, increased imaging depth was achieved over time; 1-day post-injection, signals were observed at a maximum 3-mm tissue depth, whereas 2 days post-injection, signals were observed at 4-mm tissue depth. This is presumably due to increased tumor penetration by the nanoparticles over time.

Developing novel nanomaterials that can be imaged with a number of different modalities can help merge the strengths and balance the limitations of various imaging technologies. An example of this in nanoscience is the development of upconverting nanoparticles (UCNPs), which have been gaining popularity as both fluorescent reporters and strong MRI contrast agents. Kircher et al. developed a three-imaging modality: the MRI, PAI, and SERS (MPR) nanoparticle. MPR has been used in glioblastoma tumor imaging in the mouse brain [191]. The MPR nanoparticle is composed of an Au core with a Raman-active label, trans-1,2-bis(4-pyridyl)-ethylene, and is coated successively in silica and gadolinium (Gd) for MRI contrast. *In-vitro* sensitivity tests in agarose showed that the MPR nanoparticle displays picomolar sensitivity when imaging with MRI and PAI, and sub-picomolar sensitivity with SERS. To test the effectiveness of MPRs as brain-tumor imaging agents, human glioblastoma cells were transplanted into mice, and MPRs were injected via the tail vein. All modalities showed co-localization of MPRs within the brain tumor, as verified by immunohistochemistry. The authors further used MPRs to guide tumor resection, including microscopic tumor extensions

detected by Raman and not visible to the naked eye. As a clinical tool, probes such as MPRs can be used with modalities such as MRI and PAI to identify tumors and guide early resection. MPRs can be used with higher sensitivity of SERS to verify microscopic clearance of smaller tumors.

## 5    Conclusions and outlook

Our comprehensive understanding of brain structure, physiology, activity, and neurochemistry hinges on pushing the boundaries of imaging the structural connectivity, long-range activity, and chemical communication and modulation of neurons. Improving our understanding of these systems through new microscopy techniques and functional probes will inform the study of complex brain functions and aberrations [192]. Deep-brain imaging requires: (i) overcoming challenges of microscopically imaging targets within a highly optically scattering medium, and (ii) concurrent development of probes that respond to selective neurochemical stimuli in the neuronal environment (Fig. 5). The tunable optical, chemical, and structural properties of nanomaterials render them useful for visualizing the physiology, structure, electrical activity, and chemical activity of the brain. Nanomaterials with such chemical and optical properties will provide the aforementioned information, because the presumed relationship between electrical action potentials (readily quantified by modern techniques) and chemical neurotransmission cannot be directly inferred. Recent work has shown that each action potential has a mere 6% probability of releasing the neurotransmitter dopamine [193], a key neurotransmitter implicated in decision-making, learning, and motor function. Aberrations in dopamine signaling result in anxiety, depression, and loss of motor function. Thus, when relying solely on the electrical signals of the brain to study brain function, we impose boundaries on the three primary dimensions with which we can study the brain: structure, electrical activity, and neurotransmission (Fig. 1). If we lack information on the neurochemical signals of the brain, it becomes difficult to link the role of neuromodulators with the other structural and action potential activity "dimensions" of the brain. Nanomaterial-based optical
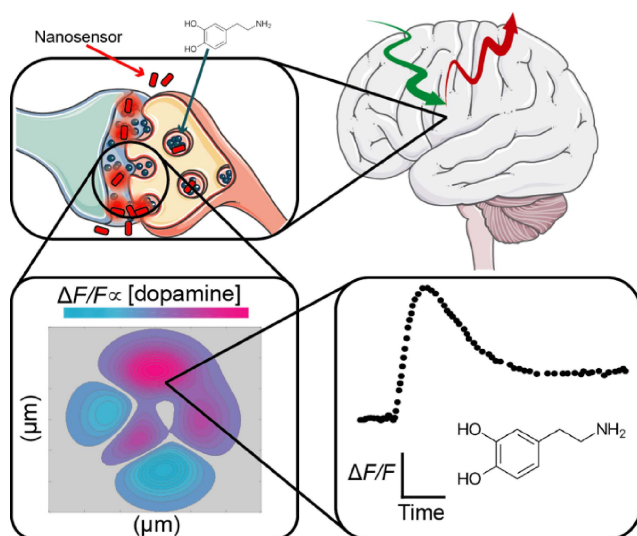
**Figure 5** The final frontier in brain imaging aims to image neurochemistry with high spatial and temporal resolution deep within the living brain. Such methods will more coherently couple and quantify the relationship between brain activity, such as neuronal firing, and neurochemical release events. This will provide important insights into chemical modulation as it relates to function, behavior, and disease.

probes will help to elucidate the "missing optical dimension" of the brain: neurochemistry. Continued development in the design and application of nano-materials for neuroimaging must focus on overcoming the challenges present in neurochemical imaging of such a complex environment. These challenges include achieving colloidal and chemical stability, biodistribution and targeting, molecular specificity, and near-infrared fluorescence. Such challenges will likely be achieved via continued engineering of the many classes of nanomaterials. Parallel advances in fluorescence microscopy will help us achieve the combined goal of deeper imaging of the structure, activity, and higher-order neurochemical function of the brain.

## Acknowledgements

## References

[1]  Kerr, J. N. D.; Denk, W. Imaging *in vivo*: Watching the brain in action. *Nat. Rev. Neurosci.* **2008**, *9*, 195–205.

[2]  Miller, E. W. Small molecule fluorescent voltage indicators for studying membrane potential. *Curr. Opin. Chem. Biol.* **2016**, *33*, 74–80.

[3]  Deo, C.; Lavis, L. D. Synthetic and genetically encoded fluorescent neural activity indicators. *Curr. Opin. Neurobiol.* **2018**, *50*, 101–108.

[4]  Patriarchi, T.; Cho, J. R.; Merten, K.; Howe, M. W.; Marley, A.; Xiong, W.-H.; Folk, R. W.; Broussard, G. J.; Liang, R. Q.; Jang M. J. et al. Ultrafast neuronal imaging of dopamine dynamics with designed genetically encoded sensors. *Science* **2018**, eaat4422.

[5]  Sun, F. M.; Zeng, J. Z.; Jing, M.; Zhou, J. H.; Feng, J. S.; Owen, S. F.; Luo, Y. C.; Li, F. N.; Yamaguchi, T.; Yong, Z. H. et al. A genetically-encoded fluorescent sensor enables rapid and specific detection of dopamine in flies, fish, and mice. *bioRxiv* **2018**, DOI: 10.1101/332528.

[6]  Kumar, A.; Tan, A. R.; Wong, J.; Spagnoli, J. C.; Lam, J.; Blevins, B. D.; Natasha, G.; Thorne, L.; Ashkan, K.; Xie, J. et al. Nanotechnology for neuroscience: Promising approaches for diagnostics, therapeutics and brain activity mapping. *Adv. Funct. Mater.* **2017**, *27*, 1700489.

[7]  Alivisatos, A. P.; Andrews, A. M.; Boyden, E. S.; Chun, M.; Church, G. M.; Deisseroth, K.; Donoghue, J. P.; Fraser, S. E.; Lippincott-Schwartz, J.; Looger, L. L. et al. Nanotools for neuroscience and brain activity mapping. *ACS Nano* **2013**, *7*, 1850–1866.

[8]  Göppert-Mayer, M. Über elementarakte mit zwei quantensprüngen. *Ann. Phys.* **1931**, *401*, 273–294.

[9]  Kaiser, W.; Garrett, C. G. B. Two-photon excitation in

CaF$_2$: Eu$^{2+}$. *Phys. Rev. Lett.* **1961**, *7*, 229–231.

[10] Denk, W.; Strickler, J. H.; Webb, W. W. Two-photon laser scanning fluorescence microscopy. *Science* **1990**, *248*, 73–76.

[11] Lakowicz, J. R. *Principles of Fluorescence Spectroscopy*, 3rd ed.; Springer-Verlag US: USA, 2006.

[12] Lefort, C. A review of biomedical multiphoton microscopy and its laser sources. *J. Phys. D: Appl. Phys.* **2017**, *50*, 423001.

[13] Sinefeld, D.; Paudel, H. P.; Ouzounov, D. G.; Bifano, T. G.; Xu, C. Adaptive optics in multiphoton microscopy: Comparison of two, three and four photon fluorescence. *Opt. Express* **2015**, *23*, 31472–31483.

[14] Sorbello, C.; Etchenique, R. Poor man's two photon imaging: Scanning laser upconversion microscopy. *bioRxiv* **2017**, DOI: 10.1101/138909.

[15] Danné, N.; Godin, A. G.; Gao, Z. H.; Varela, J. A.; Groc, L.; Lounis, B.; Cognet, L. Comparative analysis of photoluminescence and upconversion emission from individual carbon nanotubes for bioimaging applications. *ACS Photonics* **2018**, *5*, 359–364.

[16] Wang, P. Y.; Wang, C. L.; Lu, L. F.; Li, X. M.; Wang, W. X.; Zhao, M. Y.; Hu, L. D.; El-Toni, A. M.; Li, Q.; Zhang, F. Kinetics-mediate fabrication of multi-model bioimaging lanthanide nanoplates with controllable surface roughness for blood brain barrier transportation. *Biomaterials* **2017**, *141*, 223–232.

[17] Helmchen, F.; Denk, W. Deep tissue two-photon microscopy. *Nat. Methods* **2005**, *2*, 932–940.

[18] Haase, M.; Schäfer, H. Upconverting nanoparticles. *Angew. Chem., Int. Ed.* **2011**, *50*, 5808–5829.

[19] Li, S. H.; Johnson, J.; Peck, A.; Xie, Q. Near infrared fluorescent imaging of brain tumor with IR780 dye incorporated phospholipid nanoparticles. *J. Transl. Med.* **2017**, *15*, 18.

[20] Varela, J. A.; Dupuis, J. P.; Etchepare, L.; Espana, A.; Cognet, L.; Groc, L. Targeting neurotransmitter receptors with nanoparticles *in vivo* allows single-molecule tracking in acute brain slices. *Nat. Commun.* **2016**, *7*, 20947.

[21] Agarwal, R.; Domowicz, M. S.; Schwartz, N. B.; Henry, J.; Medintz, I.; Delehanty, J. B.; Stewart, M. H.; Susumu, K.; Huston, A. L.; Deschamps, J. R. et al. Delivery and tracking of quantum dot peptide bioconjugates in an intact developing avian brain. *ACS Chem. Neurosci.* **2015**, *6*, 494–504.

[22] Huang, N.; Cheng, S.; Zhang, X.; Tian, Q.; Pi, J. L.; Tang, J.; Huang, Q.; Wang, F.; Chen, J.; Xie, Z. Y. et al. Efficacy of NGR peptide-modified PEGylated quantum dots for crossing the blood–brain barrier and targeted fluorescence imaging of glioma and tumor vasculature. *Nanomed. Nanotechnol. Biol. Med.* **2017**, *13*, 83–93.

[23] Yang, H. Y.; Fu, Y.; Jang, M. S.; Li, Y.; Yin, W. P.; Ahn, T. K.; Lee, J. H.; Chae, H.; Lee, D. S. CdSe@ZnS/ZnS quantum dots loaded in polymeric micelles as a pH-triggerable targeting fluorescence imaging probe for detecting cerebral ischemic area. *Colloids Surfaces B Biointerfaces* **2017**, *155*, 497–506.

[24] Gupta, A.; Nandi, C. K. PC12 live cell ultrasensitive neurotransmitter signaling using high quantum yield sulphur doped carbon dots and its extracellular Ca$^{2+}$ ion dependence. *Sensors Actuators B Chem.* **2017**, *245*, 137–145.

[25] Romero, G.; Christiansen, M. G.; Stocche Barbosa, L.; Garcia, F.; Anikeeva, P. Localized excitation of neural activity via rapid magnetothermal drug release. *Adv. Funct. Mater.* **2016**, *26*, 6471–6478.

[26] Ruan, S. B.; Hu, C.; Tang, X.; Cun, X. L.; Xiao, W.; Shi, K. R.; He, Q.; Gao, H. L. Increased gold nanoparticle retention in brain tumors by *in situ* enzyme-induced aggregation. *ACS Nano* **2016**, *10*, 10086–10098.

[27] Tamborini, M.; Locatelli, E.; Rasile, M.; Monaco, I.; Rodighiero, S.; Corradini, I.; Comes Franchini, M.; Passoni, L.; Matteoli, M. A combined approach employing chlorotoxin-nanovectors and low dose radiation to reach infiltrating tumor niches in glioblastoma. *ACS Nano* **2016**, *10*, 2509–2520.

[28] Qian, C. G.; Zhu, S.; Feng, P. J.; Chen, Y. L.; Yu, J. C.; Tang, X.; Liu, Y.; Shen, Q. D. Conjugated polymer nanoparticles for fluorescence imaging and sensing of neurotransmitter dopamine in living cells and the brains of zebrafish larvae. *ACS Appl. Mater. Interfaces* **2015**, *7*, 18581–18589.

[29] Kobat, D.; Durst, M. E.; Nishimura, N.; Wong, A. W.; Schaffer, C. B.; Xu, C. Deep tissue multiphoton microscopy using longer wavelength excitation. *Opt. Express* **2009**, *17*, 13354–13364.

[30] Podgorski, K.; Ranganathan, G. Methods to understand brain connections and neural function: Brain heating induced by near-infrared lasers during multiphoton microscopy. *J. Neurophysiol.* **2018**, *116*, 1012–1023.

[31] Horton, N. G.; Wang, K.; Kobat, D.; Clark, C. G.; Wise, F. W.; Schaffer, C. B.; Xu, C. *In vivo* three-photon microscopy of subcortical structures within an intact mouse brain. *Nat. Photonics* **2013**, *7*, 205–209.

[32] Del Bonis-O'Donnell, J. T.; Page, R. H.; Beyene, A. G.; Tindall, E. G.; McFarlane, I. R.; Landry, M. P. Dual near-infrared two-photon microscopy for deep-tissue dopamine nanosensor imaging. *Adv. Funct. Mater.* **2017**, *27*, 1702112.

[33] Wang, J. T. W.; Rubio, N.; Kafa, H.; Venturelli, E.; Fabbro, C.; Ménard-Moyon, C.; Da Ros, T.; Sosabowski, J. K.; Lawson, A. D.; Robinson, M. K. et al. Kinetics of functionalised carbon nanotube distribution in mouse brain after systemic

injection: Spatial to ultra-structural analyses. *J. Control. Release* **2016**, *224*, 22–32.

[34] Lamy, C. M.; Sallin, O.; Loussert, C.; Chatton, J. Y. Sodium sensing in neurons with a dendrimer-based nanoprobe. *ACS Nano* **2012**, *6*, 1176–1187.

[35] Urban, B. E.; Xiao, L.; Dong, B. Q.; Chen, S. Y.; Kozorovitskiy, Y.; Zhang, H. F. Imaging neuronal structure dynamics using 2-photon super-resolution patterned excitation reconstruction microscopy. *J. Biophotonics* **2018**, *11*, e201700171.

[36] Rowlands, C. J.; Park, D.; Bruns, O. T.; Piatkevich, K. D.; Fukumura, D.; Jain, R. K.; Bawendi, M. G.; Boyden, E. S.; So, P. T. C. Wide-field three-photon excitation in biological samples. *Light Sci. Appl.* **2017**, *6*, e16255.

[37] Wang, S. W.; Xi, W.; Cai, F. H.; Zhao, X. Y.; Xu, Z. P.; Qian, J.; He, S. L. Three-photon luminescence of gold nanorods and its applications for high contrast tissue and deep *in vivo* brain imaging. *Theranostics* **2015**, *5*, 251–266.

[38] Alifu, N.; Yan, L. L.; Zhang, H. Q.; Zebibula, A.; Zhu, Z. G.; Xi, W.; Roe, A. W.; Xu, B.; Tian, W. J.; Qian, J. Organic dye doped nanoparticles with nir emission and biocompatibility for ultra-deep *in vivo* two-photon microscopy under 1040 nm femtosecond excitation. *Dye. Pigment.* **2017**, *143*, 76–85.

[39] Qian, J.; Zhu, Z. F.; Qin, A. J.; Qin, W.; Chu, L. L.; Cai, F. H.; Zhang, H. Q.; Wu, Q.; Hu, R. R.; Tang, B. Z. et al. High-order non-linear optical effects in organic luminogens with aggregation-induced emission. *Adv. Mater.* **2015**, *27*, 2332–2339.

[40] Greger, K.; Swoger, J.; Stelzer, E. H. K. Basic building units and properties of a fluorescence single plane illumination microscope. *Rev. Sci. Instrum.* **2007**, *78*, 023705.

[41] Power, R. M.; Huisken, J. A guide to light-sheet fluorescence microscopy for multiscale imaging. *Nat. Methods* **2017**, *14*, 360–373.

[42] Chen, B.-C.; Legant, W. R.; Wang, K.; Shao, L.; Milkie, D. E.; Davidson, M. W.; Janetopoulos, C.; Wu, X. S.; Hammer, J. A.; Liu, Z. et al. Lattice light-sheet microscopy: Imaging molecules to embryos at high spatiotemporal resolution. *Science* **2014**, *346*, 1257998.

[43] Wolf, S.; Supatto, W.; Debrégeas, G.; Mahou, P.; Kruglik, S. G.; Sintes, J.-M.; Beaurepaire, E.; Candelier, R. Whole-brain functional imaging with two-photon light-sheet microscopy. *Nat. Methods* **2015**, *12*, 379–380.

[44] Tomer, R.; Ye, L.; Hsueh, B.; Deisseroth, K. Advanced CLARITY for rapid and high-resolution imaging of intact tissues. *Nat. Protoc.* **2014**, *9*, 1682–1697.

[45] Stefaniuk, M.; Gualda, E. J.; Pawlowska, M.; Legutko, D.; Matryba, P.; Koza, P.; Konopka, W.; Owczarek, D.; Wawrzyniak, M.; Loza-Alvarez P, et al. Light-sheet microscopy imaging of a whole cleared rat brain with thy1-GFP transgene. *Sci. Rep.* **2016**, *6*, 28209.

[46] Wang, K.; Sun, W. Z.; Ji, N.; Betzig, E. *In vivo* brain imaging with adaptive optical microscope. In *2016 Conference on Lasers and Electro-Optics (CLEO)*, San Jose, California, USA, 2016.

[47] Tao, X.; Lin, H.; Lam, T.; Rodriguez, R.; Wang, J. W.; Kubby, J. Transcutical three-photon fluorescence imaging of drosophila brain at subcellular resolution with adaptive optics. In *Conference on Lasers and Electro-Optics*, San Jose, California, USA, 2017, pp 2–3.

[48] Chung, K.; Wallace, J.; Kim, S. Y.; Kalyanasundaram, S.; Andalman, A. S.; Davidson, T. J.; Mirzabekov, J. J.; Zalocusky, K. A.; Mattis, J.; Denisin, A. et al. Structural and molecular interrogation of intact biological systems. *Nature* **2013**, *497*, 332–337.

[49] Chung, K.; Deisseroth, K. CLARITY for mapping the nervous system. *Nat. Methods* **2013**, *10*, 508–513.

[50] Menegas, W.; Bergan, J. F.; Ogawa, S. K.; Isogai, Y.; Venkataraju, K. U.; Osten, P.; Uchida, N.; Watabe-Uchida, M. Dopamine neurons projecting to the posterior striatum form an anatomically distinct subclass. *eLife* **2015**, *4*, e10032.

[51] Ye, L.; Allen, W. E.; Thompson, K. R.; Tian, Q. Y.; Hsueh, B.; Ramakrishnan, C.; Wang, A. C.; Jennings, J. H.; Adhikari, A.; Halpem, C. H. et al. Wiring and molecular features of prefrontal ensembles representing distinct experiences. *Cell* **2016**, *165*, 1776–1788.

[52] Chen, F.; Tillberg, P. W.; Boyden, E. S. Expansion microscopy. *Science* **2015**, *347*, 543–548.

[53] Kroto, H. W.; Heath, J. R.; O'Brien, S. C.; Curl, R. F.; Smalley, R. E. C60: Buckminsterfullerene. *Nature* **1985**, *318*, 162–163.

[54] Iijima, S. Helical microtubules of graphitic carbon. *Nature* **1991**, *354*, 56–58.

[55] Novoselov, K. S.; Geim, A. K.; Morozov, S. V; Jiang, D.; Zhang, Y.; Dubonos, S. V; Grigorieva, I. V; Firsov, A. A. Electric field effect in atomically thin carbon films. *Science* **2004**, *306*, 666–669.

[56] Hirsch, A. The era of carbon allotropes. *Nat. Mater.* **2010**, *9*, 868–871.

[57] Georgakilas, V.; Perman, J. A.; Tucek, J.; Zboril, R. Broad family of carbon nanoallotropes: Classification, chemistry, and applications of fullerenes, carbon dots, nanotubes, graphene, nanodiamonds, and combined superstructures. *Chem. Rev.* **2015**, *115*, 4744–4822.

[58] Jariwala, D.; Sangwan, V. K.; Lauhon, L. J.; Marks, T. J.; Hersam, M. C. Carbon nanomaterials for electronics, optoelectronics, photovoltaics, and sensing. *Chem. Soc. Rev.* **2013**, *42*, 2824–2860.

[59] Teradal, N. L.; Jelinek, R. Carbon nanomaterials in biological studies and biomedicine. *Adv. Healthc. Mater.* **2017**, *6*, 1700574.

[60] Dai, L. M.; Chang, D. W.; Baek, J.-B.; Lu, W. Carbon nanomaterials for advanced energy conversion and storage. *Small* **2012**, *8*, 1130–1166.

[61] Mauter, M. S.; Elimelech, M. Environmental applications of carbon-based nanomaterials. *Environ. Sci. Technol.* **2008**, *42*, 5843–5859.

[62] O'Connell, M. J.; Bachilo, S. M.; Huffman, C. B.; Moore, V. C.; Strano, M. S.; Haroz, E. H.; Rialon, K. L.; Boul, P. J.; Noon, W. H.; Kittrell, C. et al. Band gap fluorescence from individual single-walled carbon nanotubes. *Science* **2002**, *297*, 593–596.

[63] Pan, D. Y.; Zhang, J. C.; Li, Z.; Wu, M. H. Hydrothermal route for cutting graphene sheets into blue-luminescent graphene quantum dots. *Adv. Mater.* **2010**, *22*, 734–738.

[64] Sun, X. M.; Liu, Z.; Welsher, K.; Robinson, J. T.; Goodwin, A.; Zaric, S.; Dai, H. J. Nano-graphene oxide for cellular imaging and drug delivery. *Nano Res.* **2008**, *1*, 203–212.

[65] Bourlinos, A. B.; Stassinopoulos, A.; Anglos, D.; Zboril, R.; Karakassides, M.; Giannelis, E. P. Surface functionalized carbogenic quantum dots. *Small* **2008**, *4*, 455–458.

[66] Kruss, S.; Hilmer, A. J.; Zhang, J. Q.; Reuel, N. F.; Mu, B.; Strano, M. S. Carbon nanotubes as optical biomedical sensors. *Adv. Drug Deliv. Rev.* **2013**, *65*, 1933–1950.

[67] Zhang, J. Q.; Landry, M. P.; Barone, P. W.; Kim, J. H.; Lin, S. C.; Ulissi, Z. W.; Lin, D. H.; Mu, B.; Boghossian, A. A.; Hilmer, A. J. et al. Molecular recognition using corona phase complexes made of synthetic polymers adsorbed on carbon nanotubes. *Nat. Nanotechnol.* **2013**, *8*, 959–968.

[68] Li, L. L.; Wu, G. H.; Yang, G. H.; Peng, J.; Zhao, J. W.; Zhu, J.-J. Focusing on luminescent graphene quantum dots: Current status and future perspectives. *Nanoscale* **2013**, *5*, 4015–4039.

[69] Hong, G. S.; Diao, S.; Antaris, A. L.; Dai, H. J. Carbon nanomaterials for biological imaging and nanomedicinal therapy. *Chem. Rev.* **2015**, *115*, 10816–10906.

[70] Kafa, H.; Wang, J. T. W.; Al-Jamal, K. T. Current perspective of carbon nanotubes application in neurology. *Int. Rev. Neurobiol.* **2016**, *130*, 229–263.

[71] Hillman, E. M. C. Optical brain imaging *in vivo*: Techniques and applications from animal to man. *J. Biomed. Opt.* **2007**, *12*, 051402.

[72] Dunn, A. K.; Wallace, V. P.; Coleno, M.; Berns, M. W.; Tromberg, B. J. Influence of optical properties on two-photon fluorescence imaging in turbid samples. *Appl. Opt.* **2000**, *39*, 1194–1201.

[73] Welsher, K.; Sherlock, S. P.; Dai, H. Deep-tissue anatomical imaging of mice using carbon nanotube fluorophores in the second near-infrared window. *Proc. Natl. Acad. Sci. USA* **2011**, *108*, 8943–8948.

[74] Heller, D. A.; Baik, S.; Eurell, T. E.; Strano, M. S. Single-walled carbon nanotube spectroscopy in live cells: Towards long-term labels and optical sensors. *Adv. Mater.* **2005**, *17*, 2793–2799.

[75] Leeuw, T. K.; Michelle Reith, R.; Simonette, R. A.; Harden, M. E.; Cherukuri, P.; Tsyboulski, D. A.; Beckingham, K. M.; Weisman, R. B. Single-walled carbon nanotubes in the intact organism: Near-IR imaging and biocompatibility studies in drosophila. *Nano Lett.* **2007**, *7*, 2650–2654.

[76] Hong, G. S.; Diao, S.; Chang, J. L.; Antaris, A. L.; Chen, C. X.; Zhang, B.; Zhao, S.; Atochin, D. N.; Huang, P. L.; Andreasson, P. L. et al. Through-skull fluorescence imaging of the brain in a new near-infrared window. *Nat. Photonics* **2014**, *8*, 723–730.

[77] Holtmaat, A.; Bonhoeffer, T.; Chow, D. K.; Chuckowree, J.; De Paola, V.; Hofer, S. B.; Hübener, M.; Keck, T.; Knott, G.; Lee, W. C. A. et al. Long-term, high-resolution imaging in the mouse neocortex through a chronic cranial window. *Nat. Protoc.* **2009**, *4*, 1128–1144.

[78] Godin, A. G.; Varela, J. A.; Gao, Z. H.; Danné, N.; Dupuis, J. P.; Lounis, B.; Groc, L.; Cognet, L. Single-nanotube tracking reveals the nanoscale organization of the extracellular space in the live brain. *Nat. Nanotechnol.* **2017**, *12*, 238–243.

[79] Syková, E.; Nicholson, C. Diffusion in brain extracellular space. *Physiol. Rev.* **2008**, *88*, 1277–1340.

[80] Vorisek, I.; Sykova, E. Measuring diffusion parameters in the brain: Comparing the real-time iontophoretic method and diffusion-weighted magnetic resonance. *Acta Physiol.* **2009**, *195*, 101–110.

[81] Vargová, L.; Syková, E. Astrocytes and extracellular matrix in extrasynaptic volume transmission. *Philos. Trans. R. Soc. Lond. B. Biol. Sci.* **2014**, *369*, 20130608.

[82] Budhathoki-Uprety, J.; Harvey, J. D.; Isaac, E.; Williams, R. M.; Galassi, T. V.; Langenbacher, R. E.; Heller, D. A. Polymer cloaking modulates the carbon nanotube protein corona and delivery into cancer cells. *J. Mater. Chem. B* **2017**, *5*, 6637–6644.

[83] Demirer, G. S.; Zhang, H.; Matos, J.; Chang, R.; Chio, L.; Staskawicz, B.; Landry, M. P. High aspect ratio nanomaterials enable biomolecule delivery and transgene expression or silencing in mature plants. *bioRxiv* **2018**, DOI: 10.1101/179549.

[84] Hong, G. S.; Wu, J. Z.; Robinson, J. T.; Wang, H. L.; Zhang, B.; Dai, H. J. Three-dimensional imaging of single nanotube molecule endocytosis on plasmonic substrates. *Nat. Commun.* **2012**, *3*, 700.

[85] Kraszewski, S.; Bianco, A.; Tarek, M.; Ramseyer, C. Insertion of short amino-functionalized single-walled carbon nanotubes into phospholipid bilayer occurs by passive diffusion. *PLoS One* **2012**, *7*, e40703.

[86] Bussy, C.; Al-Jamal, K. T.; Boczkowski, J.; Lanone, S.; Prato, M.; Bianco, A.; Kostarelos, K. Microglia determine brain region-specific neurotoxic responses to chemically functionalized carbon nanotubes. *ACS Nano* **2015**, *9*, 7815–7830.

[87] Ernst, F.; Gao, Z. H.; Arenal, R.; Heek, T.; Setaro, A.; Fernandez-Pacheco, R.; Haag, R.; Cognet, L.; Reich, S. Noncovalent Stable functionalization makes carbon nanotubes hydrophilic and biocompatible. *J. Phys. Chem. C* **2017**, *121*, 18887–18891.

[88] Landry, M. P.; Ando, H.; Chen, A. Y.; Cao, J. C.; Kottadiel, V. I.; Chio, L.; Yang, D. W.; Dong, J. Y.; Lu, T. K.; Strano, M. S. Single-molecule detection of protein efflux from microorganisms using fluorescent single-walled carbon nanotube sensor arrays. *Nat. Nanotechnol.* **2017**, *12*, 368–377.

[89] Bisker, G.; Dong, J. Y.; Park, H. D.; Iverson, N. M.; Ahn, J.; Nelson, J. T.; Landry, M. P.; Kruss, S.; Strano, M. S. Protein-targeted corona phase molecular recognition. *Nat. Commun.* **2016**, *7*, 10241.

[90] Chio, L.; Yang, D.; Landry, M. Surface engineering of nanoparticles to create synthetic antibodies. In *Synthetic Antibodies: Methods and Protocols*; Tiller, T., Ed.; Springer New York: New York, 2017; pp 363–380.

[91] Beyene, A. G.; Demirer, G. S.; Landry, M. P. Nanoparticle-templated molecular recognition platforms for detection of biological analytes. *Curr. Protoc. Chem. Biol.* **2016**, *8* 197–223.

[92] Kruss, S.; Landry, M. P.; Vander Ende, E.; Lima, B. M. A.; Reuel, N. F.; Zhang, J. Q.; Nelson, J.; Mu, B.; Hilmer, A.; Strano, M. Neurotransmitter detection using corona phase molecular recognition on fluorescent single-walled carbon nanotube sensors. *J. Am. Chem. Soc.* **2014**, *136*, 713–724.

[93] Mann, F.; Herrmann, N.; Meyer, D.; Kruss, S. Tuning selectivity of fluorescent carbon nanotube-based neurotransmitter sensors. *Sensors* **2017**, *17*, 1521.

[94] Kruss, S.; Salem, D. P.; Vuković, L.; Lima, B.; Vander Ende, E.; Boyden, E. S.; Strano, M. S. High-resolution imaging of cellular dopamine efflux using a fluorescent nanosensor array. *Proc. Natl. Acad. Sci. USA* **2017**, *114*, 1789–1794.

[95] Beyene, A. G.; Alizadehmojarad, A. A.; Dorlhiac, G.; Streets, A. M.; Kral, P.; Vuković, L.; Landry, M. P. Ultralarge modulation of single wall carbon nanotube fluorescence mediated by neuromodulators adsorbed on arrays of oligonucleotide rings. *bioRxiv* **2018**, DOI: 10.1101/351627.

[96] Beyene, A. G.; Delevich, K.; Del Bonis-O'Donnell, J. T.; Piekarski, D. J.; Lin, W. C.; Thomas, A. W.; Yang, S. J.; Kosillo, P.; Yang, D.; Wilbrecht, L. et al. Imaging striatal dopamine release using a non-genetically encoded near-infrared fluorescent catecholamine nanosensor. *bioRxiv* **2018**, DOI: 10.1101/356543.

[97] Beyene, A. G.; McFarlane, I. R.; Pinals, R. L.; Landry, M. P. Stochastic simulation of dopamine neuromodulation for implementation of fluorescent neurochemical probes in the striatal extracellular space. *ACS Chem. Neurosci.* **2017**, *8*, 2275–2289.

[98] Meyer, D.; Hagemann, A.; Kruss, S. Kinetic requirements for spatiotemporal chemical imaging with fluorescent nanosensors. *ACS Nano* **2017**, *11*, 4017–4027.

[99] Kafa, H.; Wang, J. T. W.; Rubio, N.; Venner, K.; Anderson, G.; Pach, E.; Ballesteros, B.; Preston, J. E.; Abbott, N. J.; Al-Jamal, K. T. The interaction of carbon nanotubes with an *in vitro* blood-brain barrier model and mouse brain *in vivo*. *Biomaterials* **2015**, *53*, 437–452.

[100] Shityakov, S.; Salvador, E.; Pastorin, G.; Förster, C. Blood-brain barrier transport studies, aggregation, and molecular dynamics simulation of multiwalled carbon nanotube functionalized with fluorescein isothiocyanate. *Int. J. Nanomedicine* **2015**, *10*, 1703–1713.

[101] Rubio, N.; Hirvonen, L. M.; Chong, E. Z.; Wang, J. T. W.; Bourgognon, M.; Kafa, H.; Hassan, H. A. F. M.; Al-Jamal, W. T.; McCarthy, D.; Hogstrand, C. et al. Multiphoton luminescence imaging of chemically functionalized multi-walled carbon nanotubes in cells and solid tumors. *Chem. Commun.* **2015**, *51*, 9366–9369.

[102] Cao, L.; Meziani, M. J.; Sahu, S.; Sun, Y.-P. Photoluminescence properties of graphene versus other carbon nanomaterials. *Acc. Chem. Res.* **2013**, *46*, 171–180.

[103] Miao, P.; Han, K.; Tang, Y. G.; Wang, B. D.; Lin, T.; Cheng, W. B. Recent advances in carbon nanodots: Synthesis, properties and biomedical applications. *Nanoscale* **2015**, *7*, 1586–1595.

[104] Qian, J.; Wang, D.; Cai, F.-H.; Xi, W.; Peng, L.; Zhu, Z.-F.; He, H.; Hu, M.-L.; He, S. L. Observation of multiphoton-induced fluorescence from graphene oxide nanoparticles and applications in *in vivo* functional bioimaging. *Angew. Chem., Int. Ed.* **2012**, *51*, 10570–10575.

[105] Rauti, R.; Lozano, N.; León, V.; Scaini, D.; Musto, M.; Rago, I.; Ulloa Severino, F. P.; Fabbro, A.; Casalis, L.; Vázquez, E. et al. Graphene oxide nanosheets reshape synaptic function in cultured brain networks. *ACS Nano* **2016**, *10*, 4459–4471.

[106] Lin, Y. Q.; Wang, C.; Li, L. B.; Wang, H.; Liu, K. Y.; Wang, K. Q.; Li, B. Tunable fluorescent silica-coated carbon dots: A synergistic effect for enhancing the

fluorescence sensing of extracellular $Cu^{2+}$ in rat brain. *ACS Appl. Mater. Interfaces* **2015**, *7*, 27262–27270.

[107] Baluta, S.; Cabaj, J.; Malecha, K. Neurotransmitters detection using a fluorescence-based sensor with graphene quantum dots. *Opt. Appl.* **2017**, *47*, 225–231.

[108] Mochalin, V. N.; Shenderova, O.; Ho, D.; Gogotsi, Y. The properties and applications of nanodiamonds. *Nat. Nanotechnol.* **2012**, *7*, 11–23.

[109] Haziza, S.; Mohan, N.; Loe-Mie, Y.; Lepagnol-Bestel, A.-M.; Massou, S.; Adam, M.-P.; Le, X. L.; Viard, J.; Plancon, C.; Daudin, R. et al. Fluorescent nanodiamond tracking reveals intraneuronal transport abnormalities induced by brain-disease-related genetic risk factors. *Nat. Nanotechnol.* **2017**, *12*, 322–328.

[110] Simpson, D. A.; Morrisroe, E.; McCoey, J. M.; Lombard, A. H.; Mendis, D. C.; Treussart, F.; Hall, L. T.; Petrou, S.; Hollenberg, L. C. L. Non-neurotoxic nanodiamond probes for intraneuronal temperature mapping. *ACS Nano* **2017**, *11*, 12077–12086.

[111] Hall, L. T.; Beart, G. C. G.; Thomas, E. A.; Simpson, D. A.; McGuinness, L. P.; Cole, J. H.; Manton, J. H.; Scholten, R. E.; Jelezko, F.; Wrachtrup, J. et al. High spatial and temporal resolution wide-field imaging of neuron activity using quantum NV-diamond. *Sci. Rep.* **2012**, *2*, 401.

[112] Zhang, H. L.; Aharonovich, I.; Glenn, D. R.; Schalek, R.; Magyar, A. P.; Lichtman, J. W.; Hu, E. L.; Walsworth, R. L. Silicon-vacancy color centers in nanodiamonds: Cathodoluminescence imaging markers in the near infrared. *Small* **2014**, *10*, 1908–1913.

[113] Freestone, I.; Meeks, N.; Sax, M.; Higgitt, C. The lycurgus cup - a roman nanotechnology. *Gold Bull.* **2007**, *40*, 270–277.

[114] Reed, M. A.; Bate, R. T.; Bradshaw, K.; Duncan, W. M.; Frensley, W. R.; Lee, J. W.; Shih, H. D. Spatial quantization in GaAs–AlGaAs multiple quantum dots. *J. Vac. Sci. Technol. B Microelectron. Nanom. Struct.* **1986**, *4*, 358.

[115] Pinaud, F.; Michalet, X.; Bentolila, L. A.; Tsay, J. M.; Doose, S.; Li, J. J.; Iyer, G.; Weiss, S. Advances in fluorescence imaging with quantum dot bio-probes. *Biomaterials* **2006**, *27*, 1679–1687.

[116] Alivisatos, A. P. Semiconductor clusters, nanocrystals, and quantum dots. *Science* **1996**, *271*, 933–937.

[117] Lim, Y. T.; Kim, S.; Nakayama, A.; Stott, N. E.; Bawendi, M. G.; Frangioni, J. V. Selection of quantum dot wavelengths for biomedical assays and imaging. *Mol. Imaging* **2003**, *2*, 50–64.

[118] Medintz, I. L.; Uyeda, H. T.; Goldman, E. R.; Mattoussi, H. Quantum dot bioconjugates for imaging, labelling and sensing. *Nat. Mater.* **2005**, *4*, 435–446.

[119] Smith, A.; Gao, X. H.; Nie, S. M. Quantum dot nanocrystals for *in vivo* molecular and cellular imaging? *Photochem. Photobiol.* **2004**, *80*, 377–385.

[120] Walther, C.; Meyer, K.; Rennert, R.; Neundorf, I. Quantum dot-carrier peptide conjugates suitable for imaging and delivery applications. *Bioconjugate Chem.* **2008**, *19*, 2346–2356.

[121] Zrazhevskiy, P.; Gao, X. H. Quantum dot imaging platform for single-cell molecular profiling. *Nat. Commun.* **2013**, *4*, 1619.

[122] Imamura, Y.; Yamada, S.; Tsuboi, S.; Nakane, Y.; Tsukasaki, Y.; Komatsuzaki, A.; Jin, T. Near-infrared emitting PbS quantum dots for *in vivo* fluorescence imaging of the thrombotic state in septic mouse brain. *Molecules* **2016**, *21*, 1080.

[123] Dong, B. H.; Li, C. Y.; Chen, G. C.; Zhang, Y. J.; Zhang, Y.; Deng, M. J.; Wang, Q. B. Facile synthesis of highly photoluminescent $Ag_2Se$ quantum dots as a new fluorescent probe in the second near-infrared window for *in vivo* imaging. *Chem. Mater.* **2013**, *25*, 2503–2509.

[124] Tang, R.; Xue, J. P.; Xu, B. G.; Shen, D. W.; Sudlow, G. P.; Achilefu, S. Tunable ultrasmall visible-to-extended near-infrared emitting silver sulfide quantum dots for integrin-targeted cancer imaging. *ACS Nano* **2015**, *9*, 220–230.

[125] Franke, D.; Harris, D. K.; Chen, O.; Bruns, O. T.; Carr, J. A.; Wilson, M. W. B.; Bawendi, M. G. Continuous injection synthesis of indium arsenide quantum dots emissive in the short-wavelength infrared. *Nat. Commun.* **2016**, *7*, 12749.

[126] Bruns, O. T.; Bischof, T. S.; Harris, D. K.; Franke, D.; Shi, Y. X.; Riedemann, L.; Bartelt, A.; Jaworski, F. B.; Carr, J. A.; Rowlands, C. J. et al. Next-generation *in vivo* optical imaging with short-wave infrared quantum dots. *Nat. Biomed. Eng.* **2017**, *1*, 0056.

[127] Carboni, E. J.; Bognet, B. H.; Bouchillon, G. M.; Kadilak, A. L.; Shor, L. M.; Ward, M. D.; Ma, A. W. K. Direct tracking of particles and quantification of margination in blood flow. *Biophys. J.* **2016**, *111*, 1487–1495.

[128] Saraiva, C.; Praça, C.; Ferreira, R.; Santos, T.; Ferreira, L.; Bernardino, L. Nanoparticle-mediated brain drug delivery: Overcoming blood-brain barrier to treat neurodegenerative diseases. *J. Control. Release* **2016**, *235*, 34–47.

[129] Thorne, R. G.; Nicholson, C. *In vivo* diffusion analysis with quantum dots and dextrans predicts the width of brain extracellular space. *Proc. Natl. Acad. Sci. USA* **2006**, *103*, 5567–5572.

[130] Maeda, H. The enhanced permeability and retention (EPR) effect in tumor vasculature: The key role of tumor-selective macromolecular drug targeting. *Adv. Enzyme Regul.* **2001**,

*41*, 189–207.

[131] Gao, X. L.; Chen, J.; Chen, J. Y.; Wu, B. X.; Chen, H. Z.; Jiang, X. G. Quantum dots bearing lectin-functionalized nanoparticles as a platform for *in vivo* brain imaging. *Bioconjugate Chem.* **2008**, *19*, 2189–2195.

[132] Dante, S.; Petrelli, A.; Petrini, E. M.; Marotta, R.; Maccione, A.; Alabastri, A.; Quarta, A.; De Donato, F.; Ravasenga, T.; Sathya, A. et al. Selective targeting of neurons with inorganic nanoparticles: Revealing the crucial role of nanoparticle surface Charge. *ACS Nano* **2017**, *11*, 6630–6640.

[133] Walters, R.; Medintz, I. L.; Delehanty, J. B.; Stewart, M. H.; Susumu, K.; Huston, A. L.; Dawson, P. E.; Dawson, G. The role of negative charge in the delivery of quantum dots to neurons. *ASN Neuro* **2015**, *7*, 1759091415592389.

[134] Minami, S. S.; Sun, B. G.; Popat, K.; Kauppinen, T.; Pleiss, M.; Zhou, Y. G.; Ward, M. E.; Floreancig, P.; Mucke, L.; Desai, T. et al. Selective targeting of microglia by quantum dots. *J. Neuroinflammation* **2012**, *9*, 22.

[135] Maysinger, D.; Behrendt, M.; Lalancette-Hébert, M.; Kriz, J. Real-time imaging of astrocyte response to quantum dots: *In vivo* screening model system for biocompatibility of nanoparticles. *Nano Lett.* **2007**, *7*, 2513–2520.

[136] Neuwelt, E. A.; Maravilla, K. R.; Frenkel, E. P.; Rapaport, S. I.; Hill, S. A.; Barnett, P. A. Osmotic blood-brain barrier disruption. Computerized tomographic monitoring of chemotherapeutic agent delivery. *J. Clin. Invest.* **1979**, *64*, 684–688.

[137] Pardridge, W. M. Blood-brain barrier delivery. *Drug Discov. Today* **2007**, *12*, 54–61.

[138] Larson, D. R.; Zipfel, W. R.; Williams, R. M.; Clark, S. W.; Bruchez, M. P.; Wise, F. W.; Webb, W. W. Water-soluble quantum dots for multiphoton fluorescence imaging *in vivo*. *Science* **2003**, *300*, 1434–1436.

[139] Cai, E.; Ge, P. H.; Lee, S. H.; Jeyifous, O.; Wang, Y.; Liu, Y. X.; Wilson, K. M.; Lim, S. J.; Baird, M. A.; Stone, J. E. et al. Stable small quantum dots for synaptic receptor tracking on live neurons. *Angew. Chem., Int. Ed.* **2014**, *53*, 12484–12488.

[140] Triller, A.; Choquet, D. New concepts in synaptic biology derived from single-molecule imaging. *Neuron* **2008**, *59*, 359–374.

[141] Pinaud, F.; Clarke, S.; Sittner, A.; Dahan, M. Probing cellular events, one quantum dot at a time. *Nat. Methods* **2010**, *7*, 275–285.

[142] Zhang, Q.; Li, Y.; Tsien, R. W. The dynamic control of kiss-and-run and vesicular reuse probed with single nanoparticles. *Science* **2009**, *323*, 1448–1453.

[143] Rowland, C. E.; Susumu, K.; Stewart, M. H.; Oh, E.; Mäkinen, A. J.; O'Shaughnessy, T. J.; Kushto, G.; Wolak, M. A.; Erickson, J. S.; Efros, A. et al. Electric field modulation of semiconductor quantum dot photoluminescence: Insights into the design of robust voltage-sensitive cellular imaging probes. *Nano Lett.* **2015**, *15*, 6848–6854.

[144] Marshall, J. D.; Schnitzer, M. J. Optical strategies for sensing neuronal voltage using quantum dots and other semiconductor nanocrystals. *ACS Nano* **2013**, *7*, 4601–4609.

[145] Nag, O. K.; Stewart, M. H.; Deschamps, J. R.; Susumu, K.; Oh, E.; Tsytsarev, V.; Tang, Q. G.; Efros, A. L.; Vaxenburg, R.; Black, B. J. et al. Quantum dot-peptide-fullerene bioconjugates for visualization of *in vitro* and *in vivo* cellular membrane potential. *ACS Nano* **2017**, *11*, 5598–5613.

[146] Murphy-Royal, C.; Dupuis, J. P.; Varela, J. A.; Panatier, A.; Pinson, B.; Baufreton, J.; Groc, L.; Oliet, S. H. R. Surface diffusion of astrocytic glutamate transporters shapes synaptic transmission. *Nat. Neurosci.* **2015**, *18*, 219–226.

[147] Mahendra, S.; Zhu, H. G.; Colvin, V. L.; Alvarez, P. J. Quantum dot weathering results in microbial toxicity. *Environ. Sci. Technol.* **2008**, *42*, 9424–9430.

[148] Lin, C. H.; Chang, L. W.; Chang, H.; Yang, M. H.; Yang, C. S.; Lai, W. H.; Chang, W. H.; Lin, P. P. The chemical fate of the Cd/Se/Te-based quantum dot 705 in the biological system: Toxicity implications. *Nanotechnology* **2009**, *20*, 215101.

[149] Ayoubi, M.; Naserzadeh, P.; Hashemi, M. T.; Reza Rostami, M.; Tamjid, E.; Tavakoli, M. M.; Simchi, A. Biochemical mechanisms of dose-dependent cytotoxicity and ROS-mediated apoptosis induced by lead sulfide/ graphene oxide quantum dots for potential bioimaging applications. *Sci. Rep.* **2017**, *7*, 12896.

[150] Corazzari, I.; Gilardino, A.; Dalmazzo, S.; Fubini, B.; Lovisolo, D. Localization of CdSe/ZnS quantum dots in the lysosomal acidic compartment of cultured neurons and its impact on viability: Potential role of ion release. *Toxicol. Vitr.* **2013**, *27*, 752–759.

[151] Fan, J. J.; Wang, S. F.; Zhang, X. Y.; Chen, W.; Li, Y. B.; Yang, P.; Cao, Z. L.; Wang, Y. C.; Lu, W. Y.; Ju, D. W. Quantum dots elicit hepatotoxicity through lysosome-dependent autophagy activation and reactive oxygen species production. *ACS Biomater. Sci. Eng.* **2018**, *4*, 1418–1427.

[152] Shukla, R.; Bansal, V.; Chaudhary, M.; Basu, A.; Bhonde, R. R.; Sastry, M. Biocompatibility of gold nanoparticles and their endocytotic fate inside the cellular compartment: A microscopic overview. *Langmuir* **2005**, *21*, 10644–10654.

[153] Pauksch, L.; Hartmann, S.; Rohnke, M.; Szalay, G.; Alt, V.; Schnettler, R.; Lips, K. S. Biocompatibility of silver nanoparticles and silver ions in primary human

mesenchymal stem cells and osteoblasts. *Acta Biomater.* **2014**, *10*, 439–449.

[154] Mohamed, M. B.; Volkov, V.; Link, S.; El-Sayed, M. A. The 'lightning' gold nanorods: Fluorescence enhancement of over a million compared to the gold metal. *Chem. Phys. Lett.* **2000**, *317*, 517–523.

[155] Boisselier, E.; Astruc, D. Gold nanoparticles in nanomedicine: Preparations, imaging, diagnostics, therapies and toxicity. *Chem. Soc. Rev.* **2009**, *38*, 1759–1782.

[156] Betzer, O.; Perets, N.; Angel, A.; Motiei, M.; Sadan, T.; Yadid, G.; Offen, D.; Popovtzer, R. *In vivo* neuroimaging of exosomes using gold nanoparticles. *ACS Nano* **2017**, *11*, 10883–10893.

[157] Fazaeli, Y.; Akhavan, O.; Rahighi, R.; Reza-Aboudzadeh, M.; Karimi, E.; Afarideh, H. *In vivo* SPECT imaging of tumors by [198,199]Au-labeled graphene oxide nanostructures. *Mater. Sci. Eng. C* **2014**, *45*, 196–204.

[158] Shin, T.-H.; Choi, Y.; Kim, S.; Cheon, J. Recent advances in magnetic nanoparticle-based multi-modal imaging. *Chem. Soc. Rev.* **2015**, *44*, 4501–4516.

[159] Mieszawska, A. J.; Mulder, W. J. M.; Fayad, Z. A.; Cormode, D. P. Multifunctional gold nanoparticles for diagnosis and therapy of disease. *Mol. Pharmaceutics* **2013**, *10*, 831–847.

[160] Xie, J.; Lee, S.; Chen, X. Y. Nanoparticle-based theranostic agents. *Adv. Drug Deliv. Rev.* **2010**, *62*, 1064–1079.

[161] Sonavane, G.; Tomoda, K.; Makino, K. Biodistribution of colloidal gold nanoparticles after intravenous administration: Effect of particle size. *Colloids Surfaces B Biointerfaces* **2008**, *66*, 274–280.

[162] Raliya, R.; Saha, D.; Chadha, T. S.; Raman, B.; Biswas, P. Non-invasive aerosol delivery and transport of gold nanoparticles to the brain. *Sci. Rep.* **2017**, *7*, 44718.

[163] Cheng, Y.; Meyers, J. D.; Agnes, R. S.; Doane, T. L.; Kenney, M. E.; Broome, A. M.; Burda, C.; Basilion, J. P. Addressing brain tumors with targeted gold nanoparticles: A new gold standard for hydrophobic drug delivery? *Small* **2011**, *7*, 2301–2306.

[164] Wang, H.; Huff, T. B.; Zweifel, D. A.; He, W.; Low, P. S.; Wei, A.; Cheng, J.-X. *In vitro* and *in vivo* two-photon luminescence imaging of single gold nanorods. *Proc. Natl. Acad. Sci. USA* **2005**, *102*, 15752–15756.

[165] Díez, I.; Ras, R. H. A. Fluorescent silver nanoclusters. *Nanoscale* **2011**, *3*, 1963–1970.

[166] Choi, S.; Dickson, R. M.; Yu, J. H. Developing luminescent silver nanodots for biological applications. *Chem. Soc. Rev.* **2012**, *41*, 1867–1891.

[167] Del Bonis-O'Donnell, J. T.; Thakrar, A.; Hirschberg, J. W.; Vong, D.; Queenan, B. N.; Fygenson, D. K.; Pennathur, S. DNA-stabilized silver nanoclusters as specific, ratiometric fluorescent dopamine sensors. *ACS Chem. Neurosci.* **2018**, *9*, 849–857.

[168] Akbarzadeh, A.; Rezaei-Sadabady, R.; Davaran, S.; Joo, S. W.; Zarghami, N.; Hanifehpour, Y.; Samiei, M.; Kouhi, M.; Nejati-Koshki, K. Liposome: Classification, preparation, and applications. *Nanoscale Res. Lett.* **2013**, *8*, 102.

[169] Chan, J. M.; Valencia, P. M.; Zhang, L. F.; Langer, R.; Farokhzad, O. C. Polymeric nanoparticles for drug delivery. In *Cancer Nanotechnology*; Grobmyer, S.; Moudgil, B., Eds.; Humana Press: New York, 2010; pp 163–175.

[170] Peng, H.-S.; Chiu, D. T. Soft fluorescent nanomaterials for biological and biomedical imaging. *Chem. Soc. Rev.* **2015**, *44*, 4699–4722.

[171] Metselaar, J. M.; Bruin, P.; De Boer, L. W. T.; De Vringer, T.; Snel, C.; Oussoren, C.; Wauben, M. H. M.; Crommelin, D. J. A.; Storm, G.; Hennink, W. E. A novel family of L-amino acid-based biodegradable polymer-lipid conjugates for the development of long-circulating liposomes with effective drug-targeting capacity. *Bioconjugate Chem.* **2003**, *14*, 1156–1164.

[172] Nance, E. A.; Woodworth, G. F.; Sailor, K. A.; Shih, T.-Y.; Xu, Q. G.; Swaminathan, G.; Xiang, D.; Eberhart, C.; Hanes, J. A dense poly(ethylene glycol) coating improves penetration of large polymeric nanoparticles within brain tissue. *Sci. Transl. Med.* **2012**, *4*, 149ra119.

[173] Torchilin, V. P. Recent advances with liposomes as pharmaceutical carriers. *Nat. Rev. Drug Discov.* **2005**, *4*, 145–160.

[174] Kilin, V. N.; Anton, H.; Anton, N.; Steed, E.; Vermot, J.; Vandamme, T. F.; Mely, Y.; Klymchenko, A. S. Counterion-enhanced cyanine dye loading into lipid nano-droplets for single-particle tracking in zebrafish. *Biomaterials* **2014**, *35*, 4950–4957.

[175] Wellbourne-Wood, J.; Rimmele, T. S.; Chatton, J.-Y. Imaging extracellular potassium dynamics in brain tissue using a potassium-sensitive nanosensor. *Neurophotonics* **2017**, *4*, 015002.

[176] Richers, M. T.; Amatrudo, J. M.; Olson, J. P.; Ellis-Davies, G. C. R. Cloaked caged compounds: Chemical probes for two-photon optoneurobiology. *Angew. Chem., Int. Ed.* **2017**, *56*, 193–197.

[177] Albertazzi, L.; Gherardini, L.; Brondi, M.; Sulis Sato, S.; Bifone, A.; Pizzorusso, T.; Ratto, G. M.; Bardi, G. *In vivo* distribution and toxicity of PAMAM dendrimers in the central nervous system depend on their surface chemistry. *Mol. Pharmaceutics* **2013**, *10*, 249–260.

[178] Shakhbazau, A.; Mishra, M.; Chu, T. H.; Brideau, C.; Cummins, K.; Tsutsui, S.; Shcharbin, D.; Majoral, J. P.;

Mignani, S.; Blanchard-Desce, M. et al. Fluorescent phosphorus dendrimer as a spectral nanosensor for macrophage polarization and fate tracking in spinal cord injury. *Macromol. Biosci.* **2015**, *15*, 1523–1534.

[179] Choi, H. S.; Liu, W. H.; Misra, P.; Tanaka, E.; Zimmer, J. P.; Itty Ipe, B.; Bawendi, M. G.; Frangioni, J. V. Renal clearance of quantum dots. *Nat. Biotechnol.* **2007**, *25*, 1165–1170.

[180] Ding, S. Y.; You, E. M.; Tian, Z. Q.; Moskovits, M. Electromagnetic theories of surface-enhanced Raman spectroscopy. *Chem. Soc. Rev.* **2017**, *46*, 4042–4076.

[181] Yamazoe, S.; Naya, M.; Shiota, M.; Morikawa, T.; Kubo, A.; Tani, T.; Hishiki, T.; Horiuchi, T.; Suematsu, M.; Kajimura, M. Large-area surface-enhanced Raman spectroscopy imaging of brain ischemia by gold nanoparticles grown on random nanoarrays of transparent boehmite. *ACS Nano* **2014**, *8*, 5622–5632.

[182] Wang, Y. L.; Seebald, J. L.; Szeto, D. P.; Irudayaraj, J. Biocompatibility and biodistribution of surface-enhanced Raman scattering nanoprobes in zebrafish embryos: *In vivo* and multiplex imaging. *ACS Nano* **2010**, *4*, 4039–4053.

[183] Diaz, R. J.; McVeigh, P. Z.; O'Reilly, M. A.; Burrell, K.; Bebenek, M.; Smith, C.; Etame, A. B.; Zadeh, G.; Hynynen, K.; Wilson, B. C. et al. Focused ultrasound delivery of Raman nanoparticles across the blood-brain barrier: Potential for targeting experimental brain tumors. *Nanomed. Nanotechnol. Biol. Med.* **2014**, *10*, e1075–e1087.

[184] Karabeber, H.; Huang, R. M.; Iacono, P.; Samii, J. M.; Pitter, K.; Holland, E. C.; Kircher, M. F. Guiding brain tumor resection using surface-enhanced Raman scattering nanoparticles and a hand-held Raman scanner. *ACS Nano* **2014**, *8*, 9755–9766.

[185] Huang, R. M.; Harmsen, S.; Samii, J. M.; Karabeber, H.; Pitter, K. L.; Eric, C.; Kircher, M. F. High precision imaging of microscopic spread of glioblastoma with a targeted ultrasensitive SERRS molecular imaging probe. *Theranostics* **2016**, *6*, 1075–1084.

[186] Machtoub, L.; Bataveljić, D.; Andjus, P. R. Molecular imaging of brain lipid environment of lymphocytes in amyotrophic lateral sclerosis using magnetic resonance imaging and SECARS microscopy. *Physiol. Res.* **2011**, *60*, S121–S127.

[187] Xia, J.; Yao, J.; Wang, L. V. Photoacoustic tomography: Principles and advances (invited review). *Electromagn. Waves* **2014**, *147*, 1–22.

[188] Lu, W.; Huang, Q.; Ku, G.; Wen, X. X.; Zhou, M.; Guzatov, D.; Brecht, P.; Su, R.; Oraevsky, A.; Wang, L. V. et al. Photoacoustic imaging of living mouse brain vasculature using hollow gold nanospheres. *Biomaterials* **2010**, *31*, 2617–2626.

[189] Ray, A.; Wang, X. D.; Lee, Y. K.; Hah, H. J.; Kim, G.; Chen, T.; Orringer, D. A.; Sagher, O.; Liu, X. J.; Kopelman, R. Targeted blue nanoparticles as photoacoustic contrast agent for brain tumor delineation. *Nano Res.* **2011**, *4*, 1163–1173.

[190] Fan, Q. L.; Cheng, K.; Yang, Z.; Zhang, R. P.; Yang, M.; Hu, X.; Ma, X. W.; Bu, L. H.; Lu, X. M.; Xiong, X. X. et al. Perylene-diimide-based nanoparticles as highly efficient photoacoustic agents for deep brain tumor imaging in living mice. *Adv. Mater.* **2015**, *27*, 843–847.

[191] Kircher, M. F.; De La Zerda, A.; Jokerst, J. V.; Zavaleta, C. L.; Kempen, P. J.; Mittra, E.; Pitter, K.; Huang, R. M.; Campos, C.; Habte, F. et al. A brain tumor molecular imaging strategy using a new triple-modality MRI-photoacoustic-Raman nanoparticle. *Nat. Med.* **2012**, *18*, 829–834.

[192] Kim, S. M.; Jeong, C. H.; Woo, J. S.; Ryu, C. H.; Lee, J.-H.; Jeun, S.-S. *In vivo* near-infrared imaging for the tracking of systemically delivered mesenchymal stem cells: Tropism for brain tumors and biodistribution. *Int. J. Nanomedicine* **2016**, *11*, 13–23.

[193] Pereira, D. B.; Schmitz, Y.; Mészáros, J.; Merchant, P.; Hu, G.; Li, S.; Henke, A.; Lizardi-Ortiz, J. E.; Karpowicz, R. J.; Morgenstern, T. J. et al. fluorescent false neurotransmitter reveals functionally silent dopamine vesicle clusters in the striatum. *Nat. Neurosci.* **2016**, *19*, 578–586.

# Table of contents
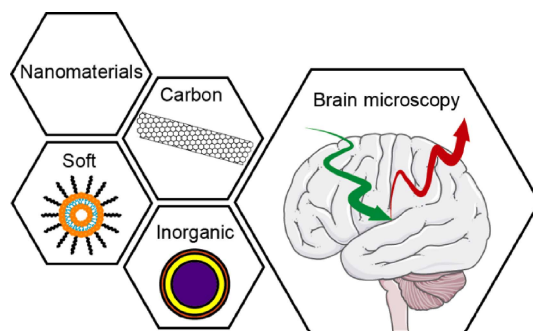


Nanomaterials are providing new insights into the structure and function of the brain. In this review, we summarize the different techniques used in optical microscopy and discuss recent advances in nanomaterials, which are enabling new methods for visualizing the living brain.